# Multi-omics and spatial mapping characterizes human CD8$^+$ T cell states in cancer

**Overline:** CANCER

**One Sentence Summary:** Tumor reactivity-driven exhausted CD8$^+$ T cells and tolerized CD8$^+$ T cells associate with contrasting immunotherapy responses in human cancers.

**Editor's Summary:** Interrogating T cells. Responses to cancer immunotherapy regimens depend on a number of factors, including the T cells and the cancer cells themselves. Here, Naulaerts *et al.* compared CD8$^+$ T cell phenotypes across multiple cancer types to identify features that associated with those tumors. CD8$^+$ T cells in immunogenic cancers such as melanoma and lung adenocarcinoma tended to have traditional exhaustion signatures. In contrast, CD8$^+$ T cells in glioblastoma were enriched for a distinct hypofunctional state. The authors investigated clinical trial data to further highlight these differences and also showed that a dendritic cell vaccine may correct the hypofunctional CD8$^+$ T cell state observed in glioblastoma. Together, these results provide insight into CD8$^+$ T cell phenotypes in the context of human cancer. -CM

# Multi-omics and spatial mapping characterizes human CD8$^+$ T cell states in cancer

Stefan Naulaerts,[1,2,3,†] Angeliki Datsi,[4,†] Daniel M Borras,[1,†] Asier Antoranz Martinez,[5,†] Julie Messiaen,[5] Isaure Vanmeerbeek,[1] Jenny Sprooten,[1] Raquel S Laureano,[1] Jannes Govaerts,[1] Dena Panovska,[5] Marleen Derweduwe,[5] Michael C. Sabel,[6] Marion Rapp,[6] Weiming Ni,[7] Sean Mackay,[7] Yannick Van Herck,[8] Lendert Gelens,[9] Tom Venken,[10,11] Sanket More,[12] Oliver Bechter,[8] Gabriele Bergers,[13,14] Adrian Liston,[15,16,17] Steven De Vleeschouwer,[18,19,20] Benoit J Van Den Eynde,[2,3] Diether Lambrechts,[10,11] Michiel Verfaillie,[21] Francesca Bosisio,[22,†] Sabine Tejpar,[23,†] Jannie Borst,[24,†] Rüdiger V. Sorg,[4,†] Frederik De Smet,[5,†] Abhishek D Garg,[1,†,*]

[1]Laboratory of Cell Stress & Immunity, Department of Cellular & Molecular Medicine, KU Leuven, 3000 Belgium; [2]Ludwig Institute for Cancer Research, Brussels, 1200 Belgium and Nuffield Department of Clinical Medicine, University of Oxford, Oxford, OX1 4BH, United Kingdom; [3]De Duve Institute, UC Louvain, Brussels, 1200 Belgium; [4]Institute for Transplantation Diagnostics and Cell Therapeutics, Medical Faculty, Heinrich Heine University Hospital, Düsseldorf, 40225 Germany; [5]Laboratory for Precision Cancer Medicine, Translational Cell and Tissue Research, Department of Imaging & Pathology, KU Leuven, 3000 Belgium; [6]Department of Neurosurgery, Medical Faculty, Heinrich Heine University Hospital, Düsseldorf, 40225 Germany; [7]IsoPlexis Corporation, Branford, Connecticut, 06405-2801 USA; [8]Laboratory of Experimental Oncology, Department of Oncology, KU Leuven, 3000 Belgium; Department of General Medical Oncology, UZ Leuven, 3000 Belgium; [9]Laboratory of Dynamics in Biological Systems, Department of Cellular & Molecular Medicine, KU Leuven, 3000 Belgium; [10]Laboratory of Translational Genetics, Department of Human Genetics, KU Leuven, 3000 Belgium; [11]VIB Center for Cancer Biology, VIB, Leuven, 3000 Belgium; [12]Department of Cellular & Molecular Medicine, KU Leuven, 3000 Belgium; [13]Laboratory of Tumor Microenvironment and Therapeutic Resistance, Department of Oncology, VIB-Center for Cancer Biology, KU Leuven, Leuven, 3000 Belgium; [14]Department of Neurological Surgery, UCSF Comprehensive Cancer Center, UCSF, San Francisco, CA, 94143-0350 United States; [15]VIB Center for Brain and Disease Research, Leuven, 3000 Belgium; [16]Department of Microbiology and Immunology, KU Leuven, 3000 Belgium; [17]Laboratory of Lymphocyte Signalling and Development, The Babraham Institute, Cambridge, CB22 3AT UK; [18]Department of Neurosurgery, University Hospitals Leuven, Leuven, 3000 Belgium; [19]Laboratory of Experimental Neurosurgery and Neuroanatomy, Department of Neurosciences, KU Leuven, 3000 Belgium; [20]Leuven Brain

Institute (LBI), Leuven, 3000 Belgium; [21]Neurosurgery Department, Europaziekenhuizen – Cliniques de l'Europe, Sint-Elisabeth, Brussels, 1180 Belgium; [22]Translational Cell & Tissue Research, Department of Imaging & Pathology, KU Leuven, 3000 Belgium; [23]Laboratory for Molecular Digestive Oncology, Department of Oncology, KU Leuven, 3000 Belgium; [24]Department of Immunology and Oncode Institute, Leiden University Medical Center, Leiden, 2333 ZA Netherlands; [25]The Leuven Institute for Single-cell omics (LISCO), KU Leuven, Belgium; [†]These authors had equal contributions.

[*]**Correspondence:** abhishek.garg@kuleuven.be

## ABSTRACT

Clinically relevant immunological biomarkers that discriminate between diverse hypofunctional states of tumor associated $CD8^+$ T cells remain disputed. Using multi-omics analysis of $CD8^+$ T cell features across multiple patient cohorts and tumor types, we identified tumor niche-dependent exhausted and other types of hypofunctional $CD8^+$ T cell states. $CD8^+$ T cells in 'supportive' niches, like melanoma or lung cancer, exhibited features of tumor reactivity-driven exhaustion ($CD8^+$ $T_{EX}$). These included a proficient effector memory phenotype, an expanded T cell receptor (TCR) repertoire linked to effector exhaustion signaling, and a cancer relevant T cell-activating immunopeptidome, composed of largely shared cancer antigens or neoantigens. In contrast, 'non-supportive' niches, like glioblastoma, were enriched for features of hypo-functionality distinct from canonical exhaustion. This included immature or insufficiently activated T cell states, high wound healing signatures, non-expanded TCR repertoires linked to anti-inflammatory signaling, high T cell recognizable self-epitopes, and an anti-proliferative state linked to stress or pro-death responses. In situ spatial mapping of glioblastoma highlighted the prevalence of dysfunctional $CD4^+$:$CD8^+$ T cell interactions, whereas ex vivo single-cell secretome mapping of glioblastoma $CD8^+$ T cells confirmed negligible effector functionality and a pro-myeloid, wound healing-like chemokine profile. Within immuno-oncology clinical trials, anti-programmed cell death protein 1 (PD-1) immunotherapy facilitated glioblastoma's tolerogenic disparities, whereas dendritic cell (DC) vaccines partly corrected them. Accordingly, recipients of a DC vaccine for glioblastoma had high effector memory $CD8^+$ T cells and evidence of antigen-specific immunity. Collectively, we provide an atlas for assessing different $CD8^+$ T cell hypofunctional states in immunogenic versus non-immunogenic cancers.

**ONE SENTENCE SUMMARY:** Tumor reactivity-driven exhausted $CD8^+$ T cells and tolerized $CD8^+$ T cells associate with contrasting immunotherapy responses in human cancers.

## INTRODUCTION

Immune-checkpoint blockade therapies (ICBs) have revolutionized oncology *(1)*, but they have only benefited a subset of antigenic tumor types *(2)*. The typical mechanism of ICBs involves 'reinvigorating' anti-tumor effector functions of $CD8^+$ T cells *(3, 4)*. This aims to counteract tumor-induced $CD8^+$ T cell exhaustion or dysfunction *(3)* characterized by loss of effector functions and upregulation of immune-inhibitory receptors *(1, 5)*. Tumor-associated $CD8^+$ T cells exhibit heterogenous hypofunctional states *(6)*. These states broadly include a spectrum of tumor reactivity induced dysfunction or exhaustion ($CD8^+$ $T_{EX}$) *(1, 5)*. $CD8^+$ $T_{EX}$ are predominantly enriched in ICB-responsive tumors, and represent a mixture of early and late $CD8^+$ $T_{EX}$, thought to be created due to chronic T cell receptor (TCR) stimulation by tumor-relevant antigens *(1, 5)*. $CD8^+$ $T_{EX}$ show clear biomarkers in terms of effector or exhaustion signaling, memory differentiation, and positive prognostic impact *(4–6)*. Studies with ICB-responsive cancers largely capture tumor reactive exhaustion-based hypofunctional $CD8^+$ T cells *(1, 3, 5, 6)*. However, it is unclear if the hypofunctionality of $CD8^+$ T cells in ICB-nonresponsive cancers is due to $CD8^+$ $T_{EX}$ or other states *(7, 8)*. Since most ICB-nonresponsive cancers exhibit low tumor relevant antigenicity, markers of hypofunctional $CD8^+$ T cells resulting from suboptimal antigen-priming or other stimuli, may be distinct from markers of late-$CD8^+$ $T_{EX}$ *(7, 8)*. However, such hypofunctional states of $CD8^+$ T cells still need to be identified in clinical samples *(7)*.

Current biomarkers for hypofunctional $CD8^+$ T cells mainly consist of immune-inhibitory receptors, interferon (IFN)-γ signaling, or memory transcription factors *(1, 6, 9)*. However, these are not always applied in an integrated manner, thus limiting their scope and creating inconsistencies for interpretations *(1)*. This limits the ability to discriminate tumors that differentially enrich $CD8^+$ $T_{EX}$ compared to other types of hypofunctional $CD8^+$ T cells. Moreover, most studies interpret these markers in a pan-cancer manner, based on non-spatial analyses *(1, 3, 6)*. As such, these approaches underestimate the impact of local cellular communities that

can define tumor ecosystems. Thus, there is a need to assess the clinical markers associated with the different hypofunctional states of $CD8^+$ T cells in a more holistic manner.

Hence, we conducted a comprehensive exploration of clinical $CD8^+$ T cell markers, integrating tumor contexts with diverse immunogenic or antigenic profiles (>4000 patients across 6 cancer types and >40 distinct clinical cohorts). We used a series of existing and consensus $CD8^+$ T cell-signatures, to drive a multi-modal and multi-dimensional mapping of $CD8^+$ T cell landscapes across six tumor types. We initially used a vast array of publicly available patient cohorts for integrated bulk RNA sequencing (RNA-seq) immunogenomics and single-cell (sc)RNA-seq driven immunology. Thereafter, proof-of-concept analyses were driven through single-cell matched scRNA-seq and scTCR-seq data generated for this study as well as by utilizing a meta-dataset of the T cell-activating immunopeptidome. These concepts were functionally validated with original patient samples. This enabled us to precisely define divergent profiles of human tumors enriching $CD8^+$ $T_{EX}$ versus other types of hypofunctional $CD8^+$ T cells. The utility of these biomarkers for precision therapy was confirmed by interrogating bulk-tumor or single-cell transcriptomics data from clinical trials for multiple cancer types or ex vivo T cell analyses from a dendritic cell (DC) vaccination clinical trial. Thus, this work provides a roadmap for optimizing immunotherapy against tumors that enrich $CD8^+$ T cells with a tolerized-like phenotype.

## RESULTS

### A chronically sensitized $CD8^+$ T cell signature differentiates tumor reactive exhaustion from naïve and transitional $CD8^+$ T cell states.

We first needed a consensus genetic signature that identified $CD8^+$ T cell states responding to ICBs, to drive our study workflow (**Fig. 1A**). Several signatures are used in immuno-oncology to predict ICB responsiveness *(10–13)* (hereafter referred to as “I-O gene sets”; **data file S1**). Some of these can capture tumor reactivity or dysfunction/exhaustion of $CD8^+$ T cells *(11, 13)*.

However, it is unclear if they capture this at single-cell resolution *(7)*. Hence, we compared 9 I-O gene sets *(10–13)* to 21 signatures derived from recent T cell-focused single-cell transcriptomics studies with matched tumor reactivity information *(14–17)* (hereafter referred to as “tumor reactive T cell gene sets”; **data file S1**). We analyzed the extent of gene overlaps between them to understand if they redundantly captured the same markers.

The overlap between the I-O and tumor-reactive T cell gene sets, as well as amongst themselves, was limited (**fig. S1A**). Nevertheless, clusters with implicit genetic cohesion did exist for tumor-reactive T cell gene sets relevant for cytolytic activity (cluster#1) and exhaustion (cluster#2) (**fig. S1A**). However, the tumor-reactive T cell gene sets covered only 7 cancer types (**fig. S1B**), with bias toward ICB-responsive types. Hence, to select consensus genes in an unbiased fashion, we performed an analysis of clinical publications involving cancer patients and investigating markers of $CD8^+$ T cell states like exhaustion/dysfunction or anergy *(18)* (**data file S1, Supplemental materials and methods**). We derived two features, number of publications per gene or protein and different $CD8^+$ T cell states (**fig. S1C)**. At least 14 gene expression features associated with terminal exhaustion/dysfunction or senescence ($IFNG^{LOW}$, $TNF^{LOW}$, $IL\text{-}2^{LOW}$, $CD28^{LOW}$, $CD57^{HIGH}$) or exhaustion/dysfunction and anergy ($PD\text{-}1^{HIGH}$, $TIM3^{HIGH}$, $CTLA4^{HIGH}$, $LAG3^{HIGH}$, $ENTPD\text{-}1^{HIGH}$, $TIGIT^{HIGH}$, $EOMES^{HIGH}$, $TOX^{HIGH}$, $CD244^{HIGH}$) across multiple studies. These analyses covered 21 cancer types (**fig. S1D**). These 14 marker genes were most often associated with tumor-reactive T cell gene sets compared to I-O gene sets (**Fig. 1B**). Since these 14 genes largely covered pathways relevant for tumor-associated chronic sensitization of $CD8^+$ T cells *(3, 5–7)*, we assembled them together with $CD8^+$ T cell lineage markers (*CD8A/B*), to form a ‘chronically sensitized’ $CD8^+$ T ($csCD8^+$ T) cell signature.

$CD8^+$ T cell exhaustion was predominantly established in the context of chronic exposure to viral infection or tumor antigens *(1, 5)*. To understand if the $csCD8^+$ T´-cell signature can differentiate between $CD8^+$ T cell states, we utilized the following existing scRNA-seq profiles: (I) human $CD8^+$ T cells infiltrating skin cutaneous melanoma (SKCM) that exhibit naive, transitional (partial

activation preceding exhaustion/dysfunction) or tumor reactivity driven dysfunctional states *(6)*; or (II) peripheral $CD8^+$ T cells from patients with high viral loads of human immunodeficiency virus (HIV) infection over 0.3 to 27 years (1 patient per timepoint; 3 patients in total), to account for time-dependent early-to-late exhaustion *(19)*. Most genes from the $csCD8^+$ T cell signature were highly expressed in tumor-reactivity driven dysfunctional $CD8^+$ T cells than in naive or transitional cells (**Fig. 1C**). Similarly, a correlation matrix of $csCD8^+$ T cell signature genes showed the highest inter-gene correlation in tumor-reactivity driven dysfunctional $CD8^+$ T cells, signifying a tendency for co-expression or concordance (**Fig. 1D to F**).

In the HIV-induced early versus late exhaustion setting, there was a balance in expression of most genes from the $csCD8^+$ T cell signature, irrespective of early (0.3-3.5 years) or late (27 years) stages of HIV infection (**Fig. 1G**). Correlation analyses of the $csCD8^+$ T cell signature genes showed highest concordance at early stage (3.5 years) (**Fig. 1H and I**), which somewhat weakened in the later stage (27 years) (**Fig. 1J**). Altogether, this implied that anti-tumor responses or early stages of chronic viral infection create $CD8^+$ T cells with considerable transcriptomic homogeneity for these genes. Hereafter, we refer to this state as tumor-reactive dysfunction/exhaustion or $CD8^+$ $T_{EX}$.

**Tumor type influences transcriptomic heterogeneity of $CD8^+$ T cell markers.**

These results merited an analysis on whether and how tumors influence transcriptomic homogeneity of the $csCD8^+$ T cell signature. Single-cell interrogations, despite their resolution, cannot be reliably utilized for high-powered analyses. However, big omics datasets that combine clinical variables with bulk tumor transcriptome profiling, such as The Cancer Genome Atlas (TCGA), are readily available. Hence, we initially prioritized TCGA-based analyses before subsequent single-cell validation.

Immune cell estimations in bulk-RNAseq are commonly done through deconvolution approaches. Hence, we verified the alignment of the csCD8$^+$ T cell signature with various immune deconvolution methods as well as 'real' tumor-infiltrating lymphocyte (TIL) features that were derived from an existing study that used tumor hematoxylin/eosin (H&E) pathology image based deep learning from TCGA *(20)*. These included number of TIL clusters and percentage of TILs from TCGA image datasets of 6 major human cancers *(20)*. The deconvolution methods included *(21)*: CIBERSORT-ABS, CIBERSORT corrected for relative tumor leukocyte fractions (CIBERSORT-CRI), xCELL, TIMER, QUANTISEQ, MCP-COUNTER and EPIC (**fig. S1E**). Deconvoluted macrophages served as negative controls. All parameters were pooled for the above cancers and analyzed using principal component analysis (PCA) (**fig. S1E**). CIBERSORT-CRI and QUANTISEQ CD8$^+$ T cell fractions clustered more closely with tumor pathological image-derived TIL features than other methods. Whereas the csCD8$^+$ T cell signature was clustered within the "CD8$^+$ T cell zone", away from macrophages, it showed less alignment with the H&E-derived TIL features (**fig. S1E**).

This seemingly aberrant position of the csCD8$^+$ T cell signature was surprising, since this signature shares several genes with most CD8$^+$ T cell deconvolution methods (**fig. S1F**). We therefore performed an analysis with linear models to capture the total amount of variation relative to various factors such as tumor type and stage, patient race, gender, or age **(fig. S2A)**. Beyond deconvolution methods, tumor type seemed to be a major contributor to the misalignments between csCD8$^+$ T cell signature and 'real' TIL features or CD8$^+$ T cell fractions.

**Diverse CD8$^+$ T cell landscapes exist across human tumors.**

We wondered whether the influence of tumor types on CD8$^+$ T cell markers could be attributed to the heterogenous CD8$^+$ T cell landscape across human cancers. Hence, we pursued a large-scale hybrid (scRNA-seq and TCGA bulk RNA-seq) bioinformatics. To account for tumor type

variability, we prioritized 6 TCGA cancers with gradually varying immunogenicity or antigenicity: highly immunogenic and highly antigenic (SKCM, lung adenocarcinoma or LUAD, and bladder carcinoma or BLCA), marginally immunogenic but low antigenic (breast carcinoma or BRCA), and low immunogenic/antigenic (glioblastoma or GBM and ovarian cancer or OV) *(13, 22)*.

An integrated multi-cancer analysis of $CD8^+$ T cells from 15 existing scRNA-seq datasets spanning 206 patients showed that genes from the $csCD8^+$ T cell signature were relatively well-expressed and homogenous in $CD8^+$ T cells from immunogenic/antigenic tumors (**Fig. 2A**). However, in direct comparison, the signature genes showed either highly heterogenous (BRCA) or largely diminished (OV or GBM) expression in $CD8^+$ T cells for other tumors (**Fig. 2A**). These patterns were relatively retained in the bulk RNA-seq data (**Fig. 2B**).

We questioned if this heterogeneity also translated into tumor type-dependent differential alignment of $CD8^+$ T cell markers. Thus, we pursued correlation of the $csCD8^+$ T cell signature with CIBERSORT-CRI $CD8^+$ T cell fractions, relative to 11 other myeloid/lymphoid cell fractions. This arranged the 6 TCGA cancers as a continuum centered around a gradient of correlations between the $csCD8^+$ T cell signature and $CD8^+$ T cell fractions, from highly positive (SKCM) to negative (GBM) (**Fig. 2C**). Such a gradient was not visible for the other cell fractions. Importantly, a similar continuum of correlations was visible between the $csCD8^+$ T cell signature and the 9 I-O gene sets (**fig. S2B**). This continuum was also quantitatively applicable such that the amounts of lymphocyte infiltration **(fig. S2C),** and $CD8^+$ T cells, went from high tumor enrichment in SKCM and LUAD to depleted in OV and GBM (**Fig. 2D**). This also translated into a gradient of positive to negative impacts on patient's overall survival (OS), for the $csCD8^+$ T cell signature and I-O gene sets (**Fig. 2E**) as well as some of the tumor-reactive T cell gene sets (**fig. S2D**).

As correlation matrices were particularly insightful for distinguishing single-cell $CD8^+$ T cell states, we repeated these for the TCGA dataset with the $csCD8^+$ T cell-signature. The $csCD8^+$ T cell signature genes showed relatively high concordance in SKCM, LUAD, BLCA, BRCA (**Fig. 2F to I**) but this correlative cohesion was lost in OV (**Fig. 2J**) and especially GBM (**Fig. 2K**).

These results indicated a gradient of $CD8^+$ T cell landscapes across different tumor types, with immunogenic/antigenic and non-immunogenic/low antigenic tumors *(22)* exhibiting homogenous versus heterogeneous behavior for cs$CD8^+$ T cell signature genes, respectively.

**SKCM and GBM $CD8^+$ T cells exhibit contrasting single-cell trajectories for effector memory and exhaustion states.**

$CD8^+$ $T_{EX}$ highly express inhibitory receptors. Since GBM and OV-$CD8^+$ T cells did not show this, this preliminarily suggested a distinct $CD8^+$ T cell state in GBM and OV. This implied that tumors like SKCM might have a higher proportion of $CD8^+$ $T_{EX}$, whereas GBM was enriched for naive/transitional $CD8^+$ T cells or hypofunctional $CD8^+$ T cells distinct from $CD8^+$ $T_{EX}$. Therefore we pursued scRNA-seq analyses using an SKCM *(23)* and a GBM *(24)* dataset (**fig. S3**) based on two criteria: (I) Smart-Seq2 based sequencing (since it gives higher sequencing depth than 10X or Droplet methods) and (II) availability of single-cell profiles for cancer cells as well as T cells (to allow cancer cell::T cell interaction analyses).

Next, we performed T cell subpopulation annotation *(1, 3, 6, 7)* (see **data file S2 and S3** for details; **fig. S4**) coupled with single-cell trajectory network analyses. This revealed that SKCM enriched for diverse $CD4^+$ and $CD8^+$ T cell-subpopulations with distinct functional or exhaustion states (**Fig. 2L to O**). SKCM-$CD8^+$ T cell subpopulations exhibited interconnectivity between states including naive ($T_N$), resident memory ($T_{RM}$), central memory ($T_{CM}$), pre-effector memory (pre-$T_{EM}$), effector-to-exhausted transitional ($T_{EET}$-like, early $T_{EET}$ and $T_{EET}$; these cells expressed both immune-inhibitory receptor genes like *PDCD1*, *LAG3*, *CTLA4* together with effector/cytolytic genes like *TBX21*, *IFNG*, *PRF1*, *GZMA/B/K*, *CCL5*, *TNF (1, 5)*), effector memory ($T_{EM}$), effector memory re-expressing CD45RA ($T_{EMRA}$), and partially activated ($T_{PA}$) cells *(1)*. SKCM-$CD4^+$ T cells also showed diverse polarization states typically associated with immunogenic tumors such as $T_H1$, $T_H2$, regulatory ($T_{reg}$), and IFN-stimulated (**Fig. 2M**). In

contrast, GBM samples were enriched for sparsely interconnected immature ($T_{IMM}$) and immunosuppressive/invariant (*TOX*$^{HI}$CD8$^+$ $T_{INV}$, *ICOS*$^{HI}$$T_{reg}$ like) CD8$^+$ T cells, together with some hypofunctional states like pre-cytotoxic (pre-$T_{CYT}$), *TOX*$^+$*TIGIT*$^+$*GZMA/K*$^{HI}$CD8$^+$ T cells or *IL7R*$^{HI}$*GZMA*$^+$*PRF1*$^+$CD8$^+$ T cells (**Fig. 2N**), with no clear recoverability of strong effector/memory phenotypes. GBM-CD4$^+$ T cells also largely showed low functional or immuno-regulatory states (**Fig. 2O**). These observations indicated that GBM datasets were enriched for a distinct hypofunctional CD8$^+$ T cell state, along with immature CD8$^+$ T cells, whereas SKCM datasets were enriched for CD8$^+$ $T_{EX}$ states. Although GBM-CD8$^+$ T cells indeed showed little expression of effector markers, one of the essential features of hypo-functionality, they did not fit the classical CD8$^+$ $T_{EX}$ phenotype due to low expression of several immune-inhibitory receptor genes, nor the anergic CD8$^+$ T cell state since anergic and exhausted states share several key features including high expression of immune-inhibitory receptor genes *(7, 18)*.

**High antigenic versus low antigenic tumors show differences in effector signaling molecules in expander versus non-expander TCR clonotypes.**

These results suggested that CD8$^+$ $T_{EX}$ enriched in antigenic tumors might have T cell receptor (TCR) mediated activation and high tumor reactivity. However, it was not clear if the hypofunctional CD8$^+$ T cell state in lower antigenic tumors like GBM showed sufficient TCR mediated activation and tumor-reactivity or a more 'tolerized' orientation *(7)*. A tolerized CD8$^+$ T cell state refers to hypo-functionality due to heightened encounters with self-antigens, and is distinguished by lack of both effector features and TCR activation as well as increased susceptibility to apoptosis *(18)*.

To address this, we compiled a single-cell matched scRNA-seq $^+$ scTCR-seq dataset of CD8$^+$ T cells across SKCM, LUAD, BRCA, and GBM. Quality control was applied during the assembly of this dataset, which excluded existing data for OV and BLCA. This dataset integrated existing

data from 44308 intra-tumoral CD8$^+$ T cells from 44 patients, that were batch-corrected using the Combat algorithm. Both visual and quantitative assessments showed that cells were sufficiently mixed for different patients and cancer types (**Fig. 3A**).

The scTCR-seq was used to define clonotypes based on shared TCR sequences. Their relative frequency per cancer type was plotted across clonal thresholds (from 2 up to 10 cells with identical TCR sequences). The frequency of TCR clonotypes per threshold varied depending on the tumor type (**Fig. 3B**). At almost every threshold, TCR clonality of SKCM or LUAD CD8$^+$ T cells was considerably higher than BRCA or GBM CD8$^+$ T cells, with GBM CD8$^+$ T cells having the least TCR clonality (**Fig. 3B**). Between the cancer types, there was very little sharing of TCR sequences, highlighting that each tumor type enriched a unique TCR repertoire (**Fig. 3C**). The threshold of 5 cells with identical TCRs was the lowest that clearly separated all cancer types. Hence, we used the ≥5 threshold to define clonotype cells with expander (E)-TCRs versus non-expander (NE)-TCRs (**Fig. 3D**).

To understand the tumor reactivity of CD8$^+$ T cells, we pursued transcriptomic analyses for E-TCRs versus NE-TCRs for each tumor type, using previously published signatures for TCR activation versus bystander activation *(25)*, and neoantigen-associated TCR activation in CD8$^+$ T cells (NeoTCR8) *(15)*. CD8$^+$ T cells with E-TCRs in SKCM, LUAD, and BRCA were enriched for a higher NeoTCR8 signature than cells with NE-TCRs (**Fig. 3E**). In contrast, GBM-CD8$^+$ T cells exhibited no difference in enrichment for NeoTCR8 (**Fig. 3E**). Similar findings were observed for not only TCR activation (**fig. S5A**) and bystander activation (**fig. S5B**) signatures, but also the csCD8$^+$ T cell signature (**Fig. 3F**). This result highlighted that the csCD8$^+$ T cell signature captured E-TCR enrichment. Overall, these results suggested that neoantigen reactivity, as extrapolated by NeoTCR8 enrichment, better differentiated E-TCR from NE-TCR CD8$^+$ T cells in antigenic tumors like SKCM than in GBM.

To validate above observations, we did a differential gene enrichment (DGE) analysis (**Fig. 3G, data file S3**), coupled with REACTOME pathway analyses (**Fig. 3H, data file S3**), between

CD8$^+$ T cells with E-TCR versus NE-TCR, integrating all 4 tumor types. We observed that E-TCR CD8$^+$ T cells enriched the following pathways or genes connected with effector or exhaustion features (**Fig. 3H, data file S3**): IFN-γ or IFN-α/β signaling (and genes like *IFNG, OASL, TBX21*), cell cycling or mitosis, immune-inhibitory receptors (*PDCD1, ENTPD1, TIGIT, HAVCR2, LAG3, ADORA2A*), TCR signaling (with exhaustion-relevant memory transcription factor genes like *TOX, EOMES*), and interleukin (IL)-2/CD28 signaling and other pro-immunogenic (*CCL5, CXCL13, CD70*) or cytotoxicity-related genes (*FASLG, PRF1, NKG7, GZMA/B/H*). In contrast, NE-TCR CD8$^+$ T cells were enriched for pathways or genes connected with cellular dysfunction, immunosuppression, or tolerization (**Fig. 3G and H**) such as anti-inflammatory signaling involving IL-4, IL-13, ADORA2B, VEGFA-VEGFR2, PDGF (and genes like *IL4R, SOCS3, CXCL16, FOS, S1PR1, PTGER2, NT5E, FOXP3*), tolerogenic transforming growth factor (TGF)-β signaling *(5, 26)*, stress responses like starvation or pro-apoptotic pathways (with genes like *BNIP3, HSPA1L, HSPA2*), and genes related to naive CD8$^+$ T cells (*IL7R, SELL, CCR7*) *(1)*.

This necessitated an analysis of the positioning of these E-TCR and NE-TCR cells relative to the tumor types. Hence, we did a comparative enrichment analysis of E-TCR versus NE-TCR CD8$^+$ T cell-derived signatures **(data file S3)** from the DGE analyses. Signatures linked to E-TCR CD8$^+$ T cells were primarily enriched in SKCM or LUAD CD8$^+$ T cells, whereas those linked to NE-TCR CD8$^+$ T cells were enriched in BRCA or GBM CD8$^+$ T cells (**Fig. 3I**). Although these signatures were linked to relatively prolonged OS in most tumor types (especially in SKCM), they were associated with a considerably shorter OS in GBM (**Fig. 3J**). Altogether, these results demonstrated that antigenic tumors are enriched for higher amounts of E-TCR CD8$^+$ T cells (thus aligning with their preference for CD8$^+$ $T_{EX}$), whereas low antigenic tumors (particularly GBM) are enriched for higher NE-TCR CD8$^+$ T cells. This supported the tendency for GBMs to enrich for hypofunctional CD8$^+$ T cells with an apparent tolerized-like CD8$^+$ T cell state *(18, 26)*.

**SKCM and LUAD enrich for cancer relevant T cell activating immunopeptidomes, whereas GBM prioritizes higher T cell activating self-epitopes.**

SKCM and LUAD had a higher fraction of tumor reactive $CD8^+$ $T_{EX}$ than GBM. However, the dominant epitope specificity for GBM-$CD8^+$ T cells was not clear. Hence, we evaluated the $CD8^+$ T cell activating immunopeptidome. Cytotoxic T lymphocyte-relevant epitopes (≥8 amino acids) were retrieved from 101 published immuno-peptidomics studies across the above described 6 cancer types. These were further filtered for only those epitopes that activated T cells in functional assays (IFN-γ production, $^{51}Cr$ release based cytotoxicity, or degranulation assays) and were classified into antigen families (shared-cancer antigens, neo-antigens, self-epitopes, or viral antigens) based on literature. This revealed that cancer relevant, shared-cancer antigens (**Fig. 3K**) or neo-antigens (**Fig. 3L**), were pre-dominantly retrievable from SKCM or LUAD. However, GBM was predominantly enriched for T cell activating self-epitopes (**Fig. 3M**). Next, a correlation analysis was performed comparing TCR clonal diversity (Shannon entropy) and transcriptomic signatures of E-TCRs, NE-TCRs, NeoTCR8s, TCR/Bystanders, and $csCD8^+$ T cells, as well as IFN-γ scores **(data file S3)** in single-nucleotide variation (SNV) derived neoantigen high tumors from TCGA. These results highlighted a bifurcated arrangement for the six cancer types (**Fig. 3N**), going from a largely positive correlation (SKCM, LUAD, BLCA, BRCA) to negative correlation (OV, GBM). This emphasized that tumors with higher $CD8^+$ $T_{EX}$ enrichment also had a more pronounced cancer relevant immunopeptidome, whereas GBM had a relatively higher enrichment of self-epitopes. High enrichment of self-epitopes, hypo-functionality, NE-TCRs and anti-inflammatory/tolerogenic signaling together suggested preferential existence of tolerized $CD8^+$ T cells in GBM *(7, 8, 18, 27)*.

**GBM-associated CD8$^+$ T cells exhibit defects in IL-2 signaling and cell cycling.**

NE-TCR CD8$^+$ T cells were enriched for pro-apoptotic pathways, whereas E-TCR CD8$^+$ T cells were enriched for proliferative pathways like cell cycling and IL-2 signaling. An association of IL-2 and high cell cycling with TCR-activated CD8$^+$ T cells is well-established *(28)*. Considering that GBM-CD8$^+$ T cells were enriched for NE-TCRs, this suggested a lack of cell cycling and higher cell death in GBM-CD8$^+$ T cells. However, the enrichment of some of these pathways was not statistically significant. Hence, this result required cross-verification in independent scRNAseq datasets with higher transcriptomic depth.

Hence, we utilized the previous Smart-seq2 datasets for SKCM and GBM **(Fig. 2A, Fig. 2L to O, fig. S3A and B)**. Confirmatively, estimation of cell cycle (phase) scores revealed that GBM-CD8$^+$ T cells exhibit lower S/G2M scores and a higher G1 score, compared to SKCM-CD8$^+$ T cells (**Fig. 4A and B**). This suggested a lack of sufficient cell cycling in GBM-CD8$^+$ T cells. It was reported previously that T cells exhibiting a lack of cell cycling and having a pre-apoptotic state induced by IL-2 starvation exhibit a very specific gene expression signature *(29)*. GBM-CD8$^+$ T cells showed a higher association with this signature than SKCM-CD8$^+$ T cells (**Fig. 4C**), indicating a G1 phase arrest-like, pro-death phenotype in GBM-CD8$^+$ T cells.

We next used cell cycle mathematical modelling for CD8$^+$ T cells proliferating after anti-CD3 and IL-2 stimuli *(30)*. We adjusted this model's parameters to reflect the cell cycle scores computed from the Smart-seq2 cohorts and used experimentally verified kinetics of anti-CD3/IL-2 stimulated CD8$^+$ T cells as a reference point *(30)*. SKCM-CD8$^+$ T cells clustered closely with this reference point, showing high S/G2M cycling, whereas GBM-CD8$^+$ T cells failed to co-cluster and showed higher G1 persistence (**Fig. 4D**). Using another independent model *(31)*, we observed that changing G1 phase-specific reaction rates predisposed GBM-CD8$^+$ T cells to a G1-arrest phenotype (**Fig. 4E**). Thus, GBM-CD8$^+$ T cells appeared to exhibit cell cycling defects.

**GBM-CD8$^+$ T cells show higher cell death or non-proliferative immunoregulation.**

The tolerized CD8$^+$ T cell state can increase susceptibility to cell death *(4, 18)*. However, cell death is hard to establish with transcriptomic data. Hence, we re-analyzed existing proteomic mass cytometry by time of flight (CyTOF) profiles for GBM-CD8$^+$ T cells (based on 161,513 CD45$^+$CD3$^+$CD8$^+$ cells from 6 GBM samples) versus LUAD-CD8$^+$ T cells (based on 356,901 CD45$^+$CD3$^+$CD8$^+$ cells from 11 non-small cell lung cancer samples), wherein 48 proteomic immune markers and cell death staining ($^{195}$Pt-cisplatin) were available *(32)*.

We found that GBM had fewer CD8$^+$ T cells per tumor than LUAD (**fig. S6A**). LUAD-CD8$^+$ T cells exhibited diverse polarization states (**Fig. 4F, fig. S6B**) including a large proportion of mostly naive and effector cells. Of note, FOXP3 marked the immuno-regulatory phenotype *(33)*. In contrast, GBM-CD8$^+$ T cells were largely composed of non-proliferating, immuno-regulatory, dysfunctional/dying, and naive cells (**Fig. 4G, fig. S6C**). We also observed small proportions of exhausted immuno-regulatory and early immuno-regulatory cells *(33)*. Thus, LUAD-CD8$^+$ T cells exhibited a higher proportion of CD8$^+$ $T_{EX}$ cells, whereas GBM-CD8$^+$ T cells had higher tolerization-like features and non-proliferative, FOXP3$^{HIGH}$ immuno-regulatory cells *(7, 8, 27, 33)*.

**TGF-β signaling and wound healing signatures characterize T cell-cancer cell interactions in GBM.**

These results suggested that the interface of GBM-CD8$^+$ T cells with the tumor is tolerogenic. To verify this, we explored computational predictions of receptor-ligand interactions between cancer cells and CD4$^+$ or CD8$^+$ T cells using CellPhoneDB in GBM as compared to SKCM. CD4$^+$ and CD8$^+$ T cells had higher predicted interaction counts with SKCM cancer cells than GBM cancer cells (**fig. S7A**). Several cancer type-specific and overlapping/shared receptors-ligand interactions were predicted between T cells and SKCM/GBM cancer cells (**fig. S7B to E**). To prioritize the most dominant interactions for further investigation, we filtered the predicted CD8$^+$-

$CD4^+$ T cell and $CD4^+$ or $CD8^+$ T cell-cancer cell interactions through SKCM or GBM TCGA-based networking approaches. SKCM-associated interactions were characterized by effector signaling, immune regulatory receptors, TNF superfamily-associated inflammation, and wound healing (**Fig. 4H**). In GBM, these interactions were skewed toward tissue repair-inflammation, TGF-β/wound healing responses or some NK cell receptors (*KLRK1, KLRC2/3*) (**Fig. 4I**).

We next asked if the TGF-β/wound healing response was negatively correlated with $CD8^+$ T cell infiltration across cancers. To address this, we again utilized TCGA data and we estimated a ratio of the TGF-β/wound healing genetic signature *(34)* to deconvoluted $CD8^+$ T cell fractions. This ratio changed in a manner that formed a continuum across the 6 cancer types, with SKCM having the lowest ratio and GBM having the highest ratio (**Fig. 4J**). Altogether, these results emphasized a cancer type specific TGF-β/wound healing footprint.

**Evidence of $CD8^+$ T cell chronic sensitization is highest near tumoral blood vessels.**

Single-cell and bulk transcriptome data indicated that GBM had higher probability of enriching immature or tolerized $CD8^+$ T cells. However, such data could be biased due to the dissociation procedures that may or may not capture the entire tumoral immune landscape *(1, 3)*. Moreover, non-spatial analyses may overlook weakly enriched, pro-immunogenic $CD8^+$ T cell states (like $T_{EX}$), in T cell hostile tumors like GBM. Finally, it was also necessary to interrogate spatially resolved functional interactions between $CD4^+$ and $CD8^+$ T cells. We pursued two step spatial analyses: we started with proteomic analyses at single-cell resolution using multiplex immunohistochemical probing of tumor tissue (MILAN) *(35)* in our SKCM and GBM patient-cohorts. This was independently validated using IVY-GAP *(36)*, a GBM tissue anatomy-driven transcriptomic dataset. Finally, we pursued TCGA derived immuno-transcriptomic validation.

The MILAN method mapped $CD4^+$ and $CD8^+$ T cells within tumor tissue from patients with SKCM and GBM **(data file S4)** inside various anatomical niches, including (I) tumoral, peri-tumoral and

non-tumoral areas, (II) intra-tumoral non-vascular, peri-vascular, and vascular zones, and (III) (GBM-specific) hemorrhagic zones (**Fig. 5A to D, fig. S8**). We confirmed our computational observations that SKCM was enriched for higher $CD8^+$ T cell density than GBM (**Fig. 5E**). Within SKCM (but not GBM), there was an enrichment of $CD8^+$ and $CD4^+$ T cells in peri- and non-tumoral areas, whereas tumoral areas were mainly enriched for $CD8^+$ T cells (**Fig. 5F; fig. S9A to C**). Within tumoral areas, SKCM and GBM T cells preferred peri-vascular zones (**Fig. 5F, fig. S9A, D to E**). GBM-$CD4^+$ and $CD8^+$ T cells were also enriched within hemorrhagic zones (**fig. S9D and E**). $CD4^+$ T cells were closer in proximity to $CD8^+$ T cells in SKCM (**fig. S9F**).

Next, we investigated $CD8^+$ T cell activation relative to spatial distribution. We used a previously established CD69-OX40 versus TIM3-LAG3 model of phenotypic activation/exhaustion (**fig. S10A to C**) *(35)*. SKCM-$CD8^+$ T cells showed higher activation than GBM-$CD8^+$ T cells (**Fig. 5G**), irrespective of anatomical location (**fig. S11A to C**). Proximity of $CD4^+$ and $CD8^+$ T cells to each (with <20µm relative distance representing cell-to-cell contact range) increased markers of activation in SKCM-$CD8^+$ T cells, but not GBM-$CD8^+$ T cells (**Fig. 5H; fig. S11D**). SKCM-$CD8^+$ T cells were more phenotypically activated in non-/peri-tumoral areas than within the tumor (**Fig. 5I**) *(3)*. This was not observed for GBM-$CD8^+$ T cells (**Fig. 5J**). In SKCM, but not GBM, vascular zones had a higher $CD8^+$ T cell activation (**Fig. 5K and L**).

We next interrogated IVY-GAP **(Fig. 5M and N**, **fig. S12A to E)**. The GBM tumor core, invasive margin, and leading edge showed depletion of T cell markers (**Fig. 5M**). A hypofunctional profile was visible, as effector function genes failed to positively correlate with *CD8A/B* (**Fig. 5N**). An appreciable proportion of GBM-$CD4^+$ and $CD8^+$ T cell markers were associated with vascular zones, particularly in immature microvascular proliferation (MVP) areas (**Fig. 5N, fig. S12B to C**). These vascular GBM-$CD8^+$ T cells co-associated with the $CD8^+$ $T_{EX}$-like phenotype (especially within MVP) and *CD4* (**Fig. 5N**). Accordingly, these vascular zones had relatively more *IFNG* and *IL2* (**fig. S12D to E**).

Lastly, to generalize these observations to other tumor types, we pursued correlative analyses between the csCD8$^+$ T cell signature and previously published *(37)* signatures for tumor relevant immature versus mature (arterial/venous) blood vessels (**data file S5**) in TCGA. In immunogenic tumors (BLCA, LUAD, SKCM) the mature blood vessel signature correlated better with the csCD8$^+$ T cell signature; these patterns were diminished in low antigenic tumors (BRCA, OV, GBM) or even reversed (GBM) (**fig. S12F**). These patterns were consistent with GBM's behavior in IVY-GAP (**fig. S12B to E**). Thus, SKCM, but not GBM, exhibited higher spatial accessibility to T cells, a pro-lymphocytic vasculature, and higher probability of CD4$^+$-CD8$^+$ T cell contacts.

**GBM-CD8$^+$ T cells lack polyfunctionality and secrete wound healing-associated chemokines.**

Immature or tolerized CD8$^+$ T cells should not be capable of processing a strong TCR stimulus *(38)*. Thus, we assessed the functionality of GBM-CD8$^+$ T cells at single-cell resolution. We freshly isolated patient derived CD8$^+$ T cells from GBM resected tumor samples and assessed their ability to be activated following exposure to anti-CD3/anti-CD28; peripheral CD8$^+$ T cells from healthy individuals were exposed to the same conditions as a control (**Fig. 6A, data file S6**). We evaluated the ability of these CD8$^+$ T cells to secrete multiple (≥2-5) cytokines, a measure of polyfunctionality, using single-cell secretome analysis *(39)* (**Fig. 6A**). Clustering analyses of the immuno-secretomes revealed that, relative to their unstimulated counterparts, and despite identical activation stimuli, the activated PBMC-derived CD8$^+$ T cells and GBM-CD8$^+$ T cells clustered separately (**Fig. 6B**). In contrast to the polyfunctional PBMC CD8$^+$ T cells, activated GBM-CD8$^+$ T cells had very low polyfunctionality (**Fig. 6C**). Similarly, whereas PBMC CD8$^+$ T cells demonstrated a 300-fold increase in polyfunctional strength index (PSI; % polyfunctional cells multiplied by the intensities of secreted cytokines) after activation, activated GBM-CD8$^+$ T cells experienced barely a 20-fold PSI increase beyond the unstimulated condition (**Fig. 6D**). The latter PSI was not driven by secretion of effector (IFN-γ) or inflammatory (TNF)

cytokines, but by pro-myeloid chemokines like IL-8, CCL3, and CCL4 (which have redundant functions during wound healing processes *(40)*) (**Fig. 6D and E**). This contrasted with stimulated PBMC $CD8^+$ T cells that secreted functionally diverse cytokines/chemokines (**Fig. 6D and E**).

Finally, we verified whether the IFN-γ production defect in GBM-$CD8^+$ T cells was specific for direct TCR stimulus or if it also occurred after stimulation with ionomycin/PMA, and if the defect also extended to $CD45RO^+$ memory $CD8^+$ T cells. To address this, PBMC-derived $CD8^+$ T cells and GBM-$CD8^+$ T cells (patient-matched) were activated by ionomycin/PMA and analyzed for expression of CD45RO and IFN-γ. Effector memory $CD8^+CD45RO^+IFN\text{-}\gamma^+$ T cells were less frequent in the GBM-$CD8^+$ T cells than in the control PBMC-derived cells after ionomycin/PMA activation (**Fig. 6F**). Altogether, these data demonstrated a hypofunctional phenotype for most GBM-$CD8^+$ T cells that may enhance pro-myeloid cell functions.

## $CD8^+$ $T_{EX}$ and tolerized $CD8^+$ T cell features define differential ICB responses in human tumors.

We next wondered if $CD8^+T_{EX}$ and tolerized $CD8^+$ T cell-differentiating genetic signatures (e.g., cs$CD8^+$ T cell, E-TCR versus NE-TCR, TGF-β/wound healing signaling) could differentiate ICB-responsiveness of antigenic and non-antigenic tumors. We thus conducted retrospective analyses of 7 published immuno-oncology clinical trials that profiled SKCM, LUAD, BLCA, and GBM tumors across 474 patients. Transcriptomic profiling was done before treatment with anti-PD-1, anti-PDL-1, anti-CTLA-4, or a combination thereof, and overall survival (OS) was analyzed after treatment *(2, 41–45)*.

Signatures for cs$CD8^+$ T cells and E-TCR $CD8^+$ T cells, as well as the IFN-γ score predicted prolonged OS after ICB treatment in SKCM, BLCA, and LUAD (**Fig. 7A**). In contrast, the ability of the NE-TCR $CD8^+$ T cell and TGF-β/wound-healing signatures to predict OS after ICB treatment, was either inconsistent or skewed toward predicting shorter OS (**Fig. 7A**) *(2)*. Almost

all the above signatures were associated with shorter OS in patients with GBM treated with ICB (**Fig. 7A**). These predictive observations for ICB responses overlapped with prognostic observations in the TCGA (**Fig. 2E**). Altogether, these data suggest that $CD8^+$ $T_{EX}$ and tolerized $CD8^+$ T cell features are associated with different outcomes in response to ICB.

**PD-1 blocking immunotherapy facilitates tolerized $CD8^+$ T cell features in GBM.**

Since the bulk transcriptomics was done on baseline samples, it was necessary to investigate the evolution of $CD8^+$ T cell features. Therefore, we interrogated SKCM and GBM clinical trials with transcriptomic profiles collected before and after PD-1 blockade *(46, 47)*. We observed no change in $CD8^+$ T cell or wound-healing signatures in SKCM (**Fig. 7B**). Although GBM samples were associated with an increase in a $CD8^+$ T cell signature after anti-PD-1 ICB, these samples were also enriched for a tolerogenic TGF-β/wound-healing signature (**Fig. 7B**). Accordingly, the $csCD8^+$ T cell signature genes exhibited concordance in SKCM, both before and after PD-1 blockade (**Fig. 7C**); whereas in GBM, PD-1 blockade reduced, rather than improved, pre-existing discordance (**Fig. 7C**). Although the $csCD8^+$ T cell signature positively correlated with OS in SKCM after anti-PD-1 ICB (**Fig. 7D**) *(47)*, this was not observed in GBM samples; further, the signature was negatively associated with a GBM-relevant positive prognostic biomarker, O(6)-Methylguanine-DNA methyltransferase (MGMT) promoter-methylation (**Fig. 7D**) *(46)*. These patterns were consistent with our earlier findings.

Finally, we validated two major observations from above analyses using scRNA-seq data from human SKCM or GBM tumors after ICB treatment. We extracted scRNA-seq data from post-ICB treatment timepoints (PD-1/CTLA4 blockade for SKCM and PD-1 blockade for GBM), from existing clinical studies with 27 patients with SKCM *(48)* and 30 patients with GBM *(49)* (**Fig. 7E to G**). After ICB treatment, the concordance of the $csCD8^+$ T cell signature was higher in SKCM-$CD8^+$ T cells as compared to GBM-$CD8^+$ T cells (**Fig. 7F**). The TGF-β/wound-healing signature

was consistently present in all GBM cellular compartments after ICB treatment (**Fig. 7G**) but was only lowly enriched in SKCM. Thus, $CD8^+$ $T_{EX}$ enriching landscapes are primed for ICB-responsiveness, whereas this was not observed in GBM, which is a tolerized $CD8^+$ T cell enriching landscape.

**Dendritic cell (DC) vaccines may ameliorate the tolerized $CD8^+$ T cell landscape in GBM.**

It has been proposed that cellular immunotherapies may overcome T cell disparities by rejuvenating antigen-specific immunity. Indeed, sporadic success has been reported for cellular immunotherapies like DC vaccines *(50)*. We therefore asked if $CD8^+$ T cell relevant genes were facilitated by DC vaccines, better than PD-1 blockade. In a DC vaccine trial with longitudinal sampling *(51)*, compared to changes elicited by PD-1 blockade in GBM (above trial), changes elicited by DC vaccination were enriched for effector genes (such as *IFNG, IL2, TNF, and CD28*) (**Fig. 8A to C**). This indicated that DC vaccines may help to overcome the tolerized $CD8^+$ T cell landscape.

**DC vaccines induce antigen-specific immunity in patients with GBM.**

Considering that an existing GBM trial did not observe enrichment of memory T cells after anti-PD-1 ICB *(52)*, and since DC vaccines showed signs of overcoming the GBM's tolerized $CD8^+$ T cell landscape, we next asked whether DC vaccines can actually rejuvenate effector memory and antigen-specific immunity. Hence, we accessed GBM-infiltrating $CD8^+$ T cells and PBMCs from the GlioVax clinical trial (NCT03395587) *(53)*. GlioVax is a phase II trial (**Fig. 8D, data file S6**) involving patients randomized into two treatment arms: (1) standard-of-care radiotherapy and chemotherapy and (2) tumor lysate-loaded DC vaccination combined with standard-of-care. Further details of the trial and DC vaccine were previously described *(53)*.

We isolated tumor-infiltrating $CD8^+$ T cells from control and DC vaccinated patients and analyzed them by flow cytometry directly or after activation with ionomycin/PMA to quantify $CD8^+CD45RO^+IFN\text{-}\gamma^+$ effector-memory T cells (**Fig. 8D**). Importantly, unvaccinated GBM samples were not enriched for effector memory $CD8^+$ T cells, and these samples failed to upregulate IFN-γ production after activation (**Fig. 8E**). However, samples from DC vaccine recipients were enriched for effector memory $CD8^+$ T cells, which showed increased IFN-γ production upon activation (**Fig. 8E**). Finally, to confirm rejuvenation of antigen-specific immunity in DC vaccinated patients, we longitudinally isolated these patients' PBMCs and re-stimulated them with the autologous GBM tumor lysate-loaded DCs as an antigen source (**Fig. 8D**), then analyzed the samples for IFN-γ production by ELISPOT. The PBMCs isolated after DC vaccination exhibited higher IFN-γ production than those derived before any therapy (baseline), or after radiotherapy and chemotherapy (post-RC/pre-vaccination) (**Fig. 8F**). Altogether, these results indicated that DC vaccines can rejuvenate functional effector memory $CD8^+$ T cell responses and antigen-specific immunity in patients with GBM.

## DISCUSSION

Our study revealed tumor-specific immune landscapes as major players in shaping enrichment of $CD8^+$ $T_{EX}$ or tolerized $CD8^+$ T cells *(1)*. $CD8^+$ $T_{EX}$ were largely enriched in immunogenic and antigenic tumors (like SKCM or LUAD) and showed transcriptional homogeneity for major T cell pathways, a positive association with outcome, high effector and co-stimulatory signaling with tumor-reactive TCR clonality and a pro-effector TCR repertoire, enrichment of a cancer relevant T cell activating immunopeptidome, stable effector memory and exhaustion states, spatially T cell-accessible tumor margins, and sufficient availability of $CD4^+$ T cell help. The $CD8^+$ $T_{EX}$ were associated with efficacy of ICBs as a therapeutic intervention. Contrastingly, tolerized $CD8^+$ T cells could be defined as a population that is mainly enriched in immuno-privileged or low antigenic tumors (especially GBM and perhaps OV). Tolerized $CD8^+$ T cells are composed of

lowly functional or dying $CD8^+$ T cells, showing high transcriptional heterogeneity for major T cell pathways, null-to-negative associations with patient outcomes, low effector and co-stimulatory signaling with tumor hypofunctional TCR clonality and an anti-inflammatory/tolerogenic TCR state, heightened recognition of self-epitopes, unstable and non-recoverable effector memory states accompanied by immunoregulation and wound healing-like chemokine profiles, sensitization toward a tolerogenic TGF-β/wound healing and spatially non-T cell supportive tumor microenvironment (TME), low cell cycle activity and cell death, and lack of $CD4^+$ T cell interactions. Tolerized $CD8^+$ T cells in GBM seemed to be hypofunctional to TCR activation in terms of cytokine production, with tendency to even facilitate wound healing-like chemokines or effector dysfunction upon CD3/CD28-activation or PD-1 blockade. High enrichment of self-reactive epitopes, the $FOXP3^{HIGH}$ phenotype, NE-TCRs, and a non-supportive TME together suggest that the tolerized phenotype of GBM-$CD8^+$ T cells might be a result of complex TME pressures aimed at avoiding autoimmune damage *(54)*.

Additionally, we observed that, although tumor-reactive features were associated with TCR clonal expansion, the consistency of this association was cancer type dependent. More specifically, this was applicable to SKCM and LUAD but, in the case like GBM, TCR clonal expansion was instead associated with anti-inflammatory/tolerogenic or stress response signaling. Importantly, our observations of the anti-inflammatory/tolerogenic orientation for the TCR repertoire in GBM are substantiated by results from immuno-oncology clinical trials: patients with GBM that did not respond to PD-1 blockade showed higher TCR clonal diversity than those that slightly responded *(2)*. Altogether, this indicated that expanded TCR clones of $CD8^+$ T cells in antigenic tumors may be less susceptible to immunosuppression than $CD8^+$ T cell clones in non-antigenic tumors *(18)*. These results suggest that TCR clonality should be analyzed from both quantitative and qualitative angles.

Another interesting observation in GBM was the increase in TGF-β and wound-healing responses after PD-1 blockade or TCR stimulation. Tolerized T cell states are meant to avoid

autoimmunity *(5, 8, 18, 27)*. Thus, the increase in TGF-β and wound healing following PD-1 blockade in GBM, as well as the preferable secretion of wound healing-like chemokines from CD3/CD28-activated GBM-CD8$^+$ T cells, may indicate these cells' programming to avoid brain-associated auto-immunity *(5, 26)*. Henceforth, cellular immunotherapies like DC vaccines should be considered for baseline restructuring of GBM-like tumors to help generate CD8$^+$ $T_{EX}$-like cells. These therapies could create a more permissive therapeutic setting for ICB treatment.

Our study has some limitations that mandate further research. For instance, the diversity of patient datasets used by us may introduce some unanticipated heterogeneity due to differences in tumor versus metastasis sampling site, age, treatment strategy, treatment sequencing or scheduling, gender, ethnicity, or immuno-haplotypes. Also, some datasets were insufficiently powered in terms of patient numbers (e.g., HIV cohort), single-cell or immuno-peptidomics data, or clinical trial cohorts. Finally, the exact molecular overlaps or distinctions between bystander CD8$^+$ and tolerized CD8$^+$ T cell states require systematic analyses. Although high enrichment of self-antigens suggested a bystander-like orientation for tolerized GBM-CD8$^+$ T cells, yet more fundamental research is needed to understand how exactly tolerized CD8$^+$ T cells are formed in GBM.

In conclusion our study delivers unique resources and methods for differentiating CD8$^+$ $T_{EX}$ from tolerized CD8$^+$ T cells in clinical settings. We believe our study provides resources, immunological and clinical insights, and a reference map for tumor relevant CD8$^+$ T cell states in cancer, as well as a critical overview of immunotherapy deterministic factors. Overall, these findings may help guide the design of immunotherapy regimens for hard-to-treat cancers.

## MATERIALS AND METHODS:

### Study Design:

Determination of sample size was not applicable for publicly available patient cohorts. For analyses of original samples, the size was not based on specific calculations but pre-determined based on availability of appropriate biobank samples. Rules for stopping data collection were pre-determined by the publicly available data or based on existing clinical protocols as applicable. There were no deliberate data exclusions. Minor variations in patient numbers occurred for some datasets, due to differential qualitative thresholds (e.g., during stratification or data transformations) or analyses-specific qualitative cut-off constraints (e.g., non-calculable values during computational calculations or deconvolutions). However, these variations didn't create any inconsistencies within our study. Nevertheless, all such variations have been transparently recorded in the figure legends or methods section. For the non-MILAN analyses, outliers were detected using the local outlier factor, as defined in PyOD (https://pyod.readthedocs.io/en/latest/). No samples were excluded as outliers. For the MILAN analysis MFI, Z-scores were trimmed in the pre-defined [0, 5] range to avoid a strong influence of any possible outliers and a median filter was applied. For MILAN-based activation scores, z-scores were trimmed to the preset [-3,3] range. All details are provided in the corresponding methods section. Reproducibility of experimental findings was verified by either considering analyses of multiple patient samples, high number of single-cells, or ≥3 biologically independent experiments. Research participants included cancer patients, or experimental units (cell cultures, single cell readouts, image quantifications, fluorescence). The overall design depending on the analyses was either controlled laboratory experiment, observational study, or survey. Please see **Fig. 1A** for an overview of our study design. As applicable, patients were randomly allocated. For in situ or ex vivo analyses, the patient samples were randomly recruited into the study from the BioBank. The primary investigators of the study were blinded to patient or sample allocation for experimental assays and initial analyses wherever applicable. For

patient information, the study protocol was approved by the UZ Leuven/KU Leuven biobank or ethical committee of the University Hospital Düsseldorf and participants gave written informed consent. DC vaccination of GBM patients in the GlioVax trial was conducted at the University Hospital Düsseldorf with the informed consent of the patients and in agreement with Art. 37 of the Declaration of Helsinki, as well as International Conference on Harmonization - Good Clinical Practice (ICH-GCP) Guideline, German Drug Law, Good Clinical Practice Regulation (GCP-V) and applicable national and European guidelines (EudraCT-Number: 2017-000304-14, NCT03395587).

**Statistical Analysis:** Statistical details of all the analyses are reported in the figure legends or figures. In some cases, the counts or number of datapoints are described in the methods section. All the statistical tests used were always two-tailed unless otherwise mentioned. In case of all experiments, the reported measurements were taken from distinct samples and not measured repeatedly from the same sample. Gene signatures were estimated by considering the average expression of all the genes within that signature, unless otherwise mentioned. All statistical analyses or graphical representations were executed using Python version 3.7.3, R versions 4.0.1, 3.6.2, and 3.5.3 or GraphPad Prism version 8. Different package versions used in this manuscript are detailed in **data file S6**. All raw, individual-level data for experiments where n<20 are presented in **data file S7.**

**Supplementary Materials:**

Supplementary Materials and Methods

fig. S1 to S13

MDAR Reproducibility Checklist

Data file S1 to S7

**References:**


1. A. M. van der Leun, D. S. Thommen, T. N. Schumacher, CD8+ T cell states in human cancer: insights from single-cell analysis., *Nat. Rev. Cancer* **20**, 218–232 (2020).

2. J. Zhao, A. X. Chen, R. D. Gartrell, A. M. Silverman, L. Aparicio, T. Chu, D. Bordbar, D. Shan, J. Samanamud, A. Mahajan, I. Filip, R. Orenbuch, M. Goetz, J. T. Yamaguchi, M. Cloney, C. Horbinski, R. V. Lukas, J. Raizer, A. I. Rae, J. Yuan, P. Canoll, J. N. Bruce, Y. M. Saenger, P. Sims, F. M. Iwamoto, A. M. Sonabend, R. Rabadan, Immune and genomic correlates of response to anti-PD-1 immunotherapy in glioblastoma., *Nat. Med.* **25**, 462–469 (2019).

3. D. S. Thommen, T. N. Schumacher, T cell dysfunction in cancer., *Cancer Cell* **33**, 547–562 (2018).

4. I. Vanmeerbeek, D. M. Borras, J. Sprooten, O. Bechter, S. Tejpar, A. D. Garg, Early memory differentiation and cell death resistance in T cells predicts melanoma response to sequential anti-CTLA4 and anti-PD1 immunotherapy., *Genes Immun.* **22**, 108–119 (2021).

5. L. M. McLane, M. S. Abdel-Hakeem, E. J. Wherry, CD8 T cell exhaustion during chronic viral infection and cancer., *Annu. Rev. Immunol.* **37**, 457–495 (2019).

6. H. Li, A. M. van der Leun, I. Yofe, Y. Lubling, D. Gelbard-Solodkin, A. C. J. van Akkooi, M. van den Braber, E. A. Rozeman, J. B. A. G. Haanen, C. U. Blank, H. M. Horlings, E. David, Y. Baran, A. Bercovich, A. Lifshitz, T. N. Schumacher, A. Tanay, I. Amit, Dysfunctional CD8 T Cells Form a Proliferative, Dynamically Regulated Compartment within Human Melanoma., *Cell* **176**, 775–789.e18 (2019).

7. A. Chow, K. Perica, C. A. Klebanoff, J. D. Wolchok, Clinical implications of T cell exhaustion for cancer immunotherapy., *Nat. Rev. Clin. Oncol.* **19**, 775–790 (2022).

8. S. Nüssing, J. A. Trapani, I. A. Parish, Revisiting T cell tolerance as a checkpoint target for cancer immunotherapy., *Front. Immunol.* **11**, 589641 (2020).

9. J. Sprooten, A. Vankerckhoven, I. Vanmeerbeek, D. M. Borras, Y. Berckmans, R. Wouters, R. S. Laureano, T. Baert, L. Boon, C. Landolfo, A. C. Testa, D. Fischerova, C. Van Holsbeke, T. Bourne, V. Chiappa, W. Froyman, D. Schols, P. Agostinis, D. Timmerman, S. Tejpar, I. Vergote, A. Coosemans, A. D. Garg, Peripherally-driven myeloid NFkB and IFN/ISG responses predict malignancy risk, survival, and immunotherapy regime in ovarian cancer., *J. Immunother. Cancer* **9** (2021), doi:10.1136/jitc-2021-003609.

10. M. Ayers, J. Lunceford, M. Nebozhyn, E. Murphy, A. Loboda, D. R. Kaufman, A. Albright, J. D. Cheng, S. P. Kang, V. Shankaran, S. A. Piha-Paul, J. Yearley, T. Y. Seiwert, A. Ribas, T. K. McClanahan, IFN-γ–related mRNA profile predicts clinical response to PD-1 blockade, *J. Clin. Invest.* (2017).

11. N. Auslander, G. Zhang, J. S. Lee, D. T. Frederick, B. Miao, T. Moll, T. Tian, Z. Wei, S. Madan, R. J. Sullivan, G. Boland, K. Flaherty, M. Herlyn, E. Ruppin, Robust prediction of

response to immune checkpoint blockade therapy in metastatic melanoma., *Nat. Med.* **24**, 1545–1549 (2018).

12. M. S. Rooney, S. A. Shukla, C. J. Wu, G. Getz, N. Hacohen, Molecular and genetic properties of tumors associated with local immune cytolytic activity., *Cell* **160**, 48–61 (2015).

13. P. Jiang, S. Gu, D. Pan, J. Fu, A. Sahu, X. Hu, Z. Li, N. Traugh, X. Bu, B. Li, J. Liu, G. J. Freeman, M. A. Brown, K. W. Wucherpfennig, X. S. Liu, Signatures of T cell dysfunction and exclusion predict cancer immunotherapy response., *Nat. Med.* **24**, 1550–1558 (2018).

14. G. Oliveira, K. Stromhaug, S. Klaeger, T. Kula, D. T. Frederick, P. M. Le, J. Forman, T. Huang, S. Li, W. Zhang, Q. Xu, N. Cieri, K. R. Clauser, S. A. Shukla, D. Neuberg, S. Justesen, G. MacBeath, S. A. Carr, E. F. Fritsch, N. Hacohen, M. Sade-Feldman, K. J. Livak, G. M. Boland, P. A. Ott, D. B. Keskin, C. J. Wu, Phenotype, specificity and avidity of antitumour CD8+ T cells in melanoma., *Nature* **596**, 119–125 (2021).

15. F. J. Lowery, S. Krishna, R. Yossef, N. B. Parikh, P. D. Chatani, N. Zacharakis, M. R. Parkhurst, N. Levin, S. Sindiri, A. Sachs, K. J. Hitscherich, Z. Yu, N. R. Vale, Y.-C. Lu, Z. Zheng, L. Jia, J. J. Gartner, V. K. Hill, A. R. Copeland, S. K. Nah, R. V. Masi, B. Gasmi, S. Kivitz, B. C. Paria, M. Florentin, S. P. Kim, K.-I. Hanada, Y. F. Li, L. T. Ngo, S. Ray, M. L. Shindorf, S. T. Levi, R. Shepherd, C. Toy, A. Y. Parikh, T. D. Prickett, M. C. Kelly, R. Beyer, S. L. Goff, J. C. Yang, P. F. Robbins, S. A. Rosenberg, Molecular signatures of antitumor neoantigen-reactive T cells from metastatic human cancers., *Science* **375**, 877–884 (2022).

16. C. Zheng, J. N. Fass, Y.-P. Shih, A. J. Gunderson, N. Sanjuan Silva, H. Huang, B. M. Bernard, V. Rajamanickam, J. Slagel, C. B. Bifulco, B. Piening, P. H. A. Newell, P. D. Hansen, E. Tran, Transcriptomic profiles of neoantigen-reactive T cells in human gastrointestinal cancers., *Cancer Cell* **40**, 410–423.e7 (2022).

17. A. M. Luoma, S. Suo, Y. Wang, L. Gunasti, C. B. M. Porter, N. Nabilsi, J. Tadros, A. P. Ferretti, S. Liao, C. Gurer, Y.-H. Chen, S. Criscitiello, C. A. Ricker, D. Dionne, O. Rozenblatt-Rosen, R. Uppaluri, R. I. Haddad, O. Ashenberg, A. Regev, E. M. Van Allen, G. MacBeath, J. D. Schoenfeld, K. W. Wucherpfennig, Tissue-resident memory and circulating T cells are early responders to pre-surgical cancer immunotherapy., *Cell* **185**, 2918–2935.e29 (2022).

18. M. Philip, A. Schietinger, CD8+ T cell differentiation and dysfunction in cancer., *Nat. Rev. Immunol.* **22**, 209–223 (2022).

19. S. Wang, Q. Zhang, H. Hui, K. Agrawal, M. A. Y. Karris, T. M. Rana, An atlas of immune cell exhaustion in HIV-infected individuals revealed by single-cell transcriptomics., *Emerg. Microbes Infect.* **9**, 2333–2347 (2020).

20. J. Saltz, R. Gupta, L. Hou, T. Kurc, P. Singh, V. Nguyen, D. Samaras, K. R. Shroyer, T. Zhao, R. Batiste, J. Van Arnam, Cancer Genome Atlas Research Network, I. Shmulevich, A. U. K. Rao, A. J. Lazar, A. Sharma, V. Thorsson, Spatial Organization and Molecular Correlation of Tumor-Infiltrating Lymphocytes Using Deep Learning on Pathology Images., *Cell Rep.* **23**, 181–193.e7 (2018).

21. F. Finotello, D. Rieder, H. Hackl, Z. Trajanoski, Next-generation computational tools for interrogating cancer immunity., *Nat. Rev. Genet.* **20**, 724–746 (2019).

22. M. Yarchoan, A. Hopkins, E. M. Jaffee, Tumor Mutational Burden and Response Rate to PD-1 Inhibition., *N. Engl. J. Med.* **377**, 2500–2501 (2017).

23. I. Tirosh, B. Izar, S. M. Prakadan, M. H. Wadsworth, D. Treacy, J. J. Trombetta, A. Rotem, C. Rodman, C. Lian, G. Murphy, M. Fallahi-Sichani, K. Dutton-Regester, J.-R. Lin, O. Cohen, P. Shah, D. Lu, A. S. Genshaft, T. K. Hughes, C. G. K. Ziegler, S. W. Kazer, A. Gaillard, K. E. Kolb, A.-C. Villani, C. M. Johannessen, A. Y. Andreev, E. M. Van Allen, M. Bertagnolli, P. K. Sorger, R. J. Sullivan, K. T. Flaherty, D. T. Frederick, J. Jané-Valbuena, C. H. Yoon, O. Rozenblatt-Rosen, A. K. Shalek, A. Regev, L. A. Garraway, Dissecting the multicellular ecosystem of metastatic melanoma by single-cell RNA-seq., *Science* **352**, 189–196 (2016).

24. C. Neftel, J. Laffy, M. G. Filbin, T. Hara, M. E. Shore, G. J. Rahme, A. R. Richman, D. Silverbush, M. L. Shaw, C. M. Hebert, J. Dewitt, S. Gritsch, E. M. Perez, L. N. Gonzalez Castro, X. Lan, N. Druck, C. Rodman, D. Dionne, A. Kaplan, M. S. Bertalan, J. Small, K. Pelton, S. Becker, D. Bonal, Q.-D. Nguyen, R. L. Servis, J. M. Fung, R. Mylvaganam, L. Mayr, J. Gojo, C. Haberler, R. Geyeregger, T. Czech, I. Slavc, B. V. Nahed, W. T. Curry, B. S. Carter, H. Wakimoto, P. K. Brastianos, T. T. Batchelor, A. Stemmer-Rachamimov, M. Martinez-Lage, M. P. Frosch, I. Stamenkovic, N. Riggi, E. Rheinbay, M. Monje, O. Rozenblatt-Rosen, D. P. Cahill, A. P. Patel, T. Hunter, I. M. Verma, K. L. Ligon, D. N. Louis, A. Regev, B. E. Bernstein, I. Tirosh, M. L. Suvà, An integrative model of cellular states, plasticity, and genetics for glioblastoma., *Cell* **178**, 835–849.e21 (2019).

25. S. C. Bangs, D. Baban, H. J. Cattan, C. K.-F. Li, A. J. McMichael, X.-N. Xu, Human CD4+ memory T cells are preferential targets for bystander activation and apoptosis., *J. Immunol.* **182**, 1962–1971 (2009).

26. J. Y. Niederkorn, See no evil, hear no evil, do no evil: the lessons of immune privilege., *Nat. Immunol.* **7**, 354–359 (2006).

27. A. Schietinger, P. D. Greenberg, Tolerance and exhaustion: defining mechanisms of T cell dysfunction., *Trends Immunol.* **35**, 51–60 (2014).

28. S. Zenke, M. M. Palm, J. Braun, A. Gavrilov, P. Meiser, J. P. Böttcher, N. Beyersdorf, S. Ehl, A. Gerard, T. Lämmermann, T. N. Schumacher, J. B. Beltman, J. C. Rohr, Quorum Regulation via Nested Antagonistic Feedback Circuits Mediated by the Receptors CD28 and CTLA-4 Confers Robustness to T Cell Population Dynamics., *Immunity* **52**, 313–327.e7 (2020).

29. M. Chechlinska, J. K. Siwicki, M. Gos, M. Oczko-Wojciechowska, M. Jarzab, A. Pfeifer, B. Jarzab, J. Steffen, Molecular signature of cell cycle exit induced in human T lymphoblasts by IL-2 withdrawal., *BMC Genomics* **10**, 261 (2009).

30. M. R. Dowling, A. Kan, S. Heinzel, J. H. S. Zhou, J. M. Marchingo, C. J. Wellard, J. F. Markham, P. D. Hodgkin, Stretched cell cycle model for proliferating lymphocytes., *Proc. Natl. Acad. Sci. USA* **111**, 6377–6382 (2014).

31. H. X. Chao, R. I. Fakhreddin, H. K. Shimerov, K. M. Kedziora, R. J. Kumar, J. Perez, J. C. Limas, G. D. Grant, J. G. Cook, G. P. Gupta, J. E. Purvis, Evidence that the human cell cycle is a series of uncoupled, memoryless phases., *Mol. Syst. Biol.* **15**, e8604 (2019).

32. S. Goswami, T. Walle, A. E. Cornish, S. Basu, S. Anandhan, I. Fernandez, L. Vence, J. Blando, H. Zhao, S. S. Yadav, M. Ott, L. Y. Kong, A. B. Heimberger, J. de Groot, B. Sepesi, M. Overman, S. Kopetz, J. P. Allison, D. Pe'er, P. Sharma, Immune profiling of human tumors identifies CD73 as a combinatorial target in glioblastoma., *Nat. Med.* **26**, 39–46 (2020).

33. G. Churlaud, F. Pitoiset, F. Jebbawi, R. Lorenzon, B. Bellier, M. Rosenzwajg, D. Klatzmann, Human and Mouse CD8(+)CD25(+)FOXP3(+) Regulatory T Cells at Steady State and during Interleukin-2 Therapy., *Front. Immunol.* **6**, 171 (2015).

34. V. Thorsson, D. L. Gibbs, S. D. Brown, D. Wolf, D. S. Bortone, T.-H. Ou Yang, E. Porta-Pardo, G. F. Gao, C. L. Plaisier, J. A. Eddy, E. Ziv, A. C. Culhane, E. O. Paull, I. K. A. Sivakumar, A. J. Gentles, R. Malhotra, F. Farshidfar, A. Colaprico, J. S. Parker, L. E. Mose, N. S. Vo, J. Liu, Y. Liu, J. Rader, V. Dhankani, S. M. Reynolds, R. Bowlby, A. Califano, A. D. Cherniack, D. Anastassiou, D. Bedognetti, Y. Mokrab, A. M. Newman, A. Rao, K. Chen, A. Krasnitz, H. Hu, T. M. Malta, H. Noushmehr, C. S. Pedamallu, S. Bullman, A. I. Ojesina, A. Lamb, W. Zhou, H. Shen, T. K. Choueiri, J. N. Weinstein, J. Guinney, J. Saltz, R. A. Holt, C. S. Rabkin, Cancer Genome Atlas Research Network, A. J. Lazar, J. S. Serody, E. G. Demicco, M. L. Disis, B. G. Vincent, I. Shmulevich, The immune landscape of cancer., *Immunity* **48**, 812–830.e14 (2018).

35. F. M. Bosisio, A. Antoranz, Y. van Herck, M. M. Bolognesi, L. Marcelis, C. Chinello, J. Wouters, F. Magni, L. Alexopoulos, M. Stas, V. Boecxstaens, O. Bechter, G. Cattoretti, J. van den Oord, Functional heterogeneity of lymphocytic patterns in primary melanoma dissected through single-cell multiplexing., *Elife* **9** (2020), doi:10.7554/eLife.53008.

36. R. B. Puchalski, N. Shah, J. Miller, R. Dalley, S. R. Nomura, J.-G. Yoon, K. A. Smith, M. Lankerovich, D. Bertagnolli, K. Bickley, A. F. Boe, K. Brouner, S. Butler, S. Caldejon, M. Chapin, S. Datta, N. Dee, T. Desta, T. Dolbeare, N. Dotson, A. Ebbert, D. Feng, X. Feng, M. Fisher, G. Gee, J. Goldy, L. Gourley, B. W. Gregor, G. Gu, N. Hejazinia, J. Hohmann, P. Hothi, R. Howard, K. Joines, A. Kriedberg, L. Kuan, C. Lau, F. Lee, H. Lee, T. Lemon, F. Long, N. Mastan, E. Mott, C. Murthy, K. Ngo, E. Olson, M. Reding, Z. Riley, D. Rosen, D. Sandman, N. Shapovalova, C. R. Slaughterbeck, A. Sodt, G. Stockdale, A. Szafer, W. Wakeman, P. E. Wohnoutka, S. J. White, D. Marsh, R. C. Rostomily, L. Ng, C. Dang, A. Jones, B. Keogh, H. R. Gittleman, J. S. Barnholtz-Sloan, P. J. Cimino, M. S. Uppin, C. D. Keene, F. R. Farrokhi, J. D. Lathia, M. E. Berens, A. Iavarone, A. Bernard, E. Lein, J. W. Phillips, S. W. Rostad, C. Cobbs, M. J. Hawrylycz, G. D. Foltz, An anatomic transcriptional atlas of human glioblastoma., *Science* **360**, 660–663 (2018).

37. J. Goveia, K. Rohlenova, F. Taverna, L. Treps, L.-C. Conradi, A. Pircher, V. Geldhof, L. P. M. H. de Rooij, J. Kalucka, L. Sokol, M. García-Caballero, Y. Zheng, J. Qian, L.-A. Teuwen, S. Khan, B. Boeckx, E. Wauters, H. Decaluwé, P. De Leyn, J. Vansteenkiste, B. Weynand, X. Sagaert, E. Verbeken, A. Wolthuis, B. Topal, W. Everaerts, H. Bohnenberger, A. Emmert, D. Panovska, F. De Smet, F. J. T. Staal, R. J. Mclaughlin, F. Impens, V. Lagani, S. Vinckier, M. Mazzone, L. Schoonjans, M. Dewerchin, G. Eelen, T. K. Karakach, H. Yang, J. Wang, L. Bolund, L. Lin, B. Thienpont, X. Li, D. Lambrechts, Y. Luo, P. Carmeliet, An integrated gene expression landscape profiling approach to identify lung tumor endothelial cell heterogeneity and angiogenic candidates., *Cancer Cell* **37**, 21–36.e13 (2020).

38. I. Sandu, D. Cerletti, N. Oetiker, M. Borsa, F. Wagen, I. Spadafora, S. P. M. Welten, U. Stolz, A. Oxenius, M. Claassen, Landscape of Exhausted Virus-Specific CD8 T Cells in Chronic LCMV Infection., *Cell Rep.* **32**, 108078 (2020).

39. D. Liu, P. Paczkowski, S. Mackay, C. Ng, J. Zhou, Single-Cell Multiplexed Proteomics on the IsoLight Resolves Cellular Functional Heterogeneity to Reveal Clinical Responses of Cancer Patients to Immunotherapies., *Methods Mol. Biol.* **2055**, 413–431 (2020).

40. A. Ridiandries, J. T. M. Tan, C. A. Bursill, The role of chemokines in wound healing., *Int. J. Mol. Sci.* **19** (2018), doi:10.3390/ijms19103217.

41. S. Hwang, A.-Y. Kwon, J.-Y. Jeong, S. Kim, H. Kang, J. Park, J.-H. Kim, O. J. Han, S. M. Lim, H. J. An, Immune gene signatures for predicting durable clinical benefit of anti-PD-1 immunotherapy in patients with non-small cell lung cancer., *Sci. Rep.* **10**, 643 (2020).

42. N. Riaz, J. J. Havel, V. Makarov, A. Desrichard, W. J. Urba, J. S. Sims, F. S. Hodi, S. Martín-Algarra, R. Mandal, W. H. Sharfman, S. Bhatia, W.-J. Hwu, T. F. Gajewski, C. L. Slingluff, D. Chowell, S. M. Kendall, H. Chang, R. Shah, F. Kuo, L. G. T. Morris, J.-W. Sidhom, J. P. Schneck, C. E. Horak, N. Weinhold, T. A. Chan, Tumor and Microenvironment Evolution during Immunotherapy with Nivolumab., *Cell* **171**, 934–949.e16 (2017).

43. S. Mariathasan, S. J. Turley, D. Nickles, A. Castiglioni, K. Yuen, Y. Wang, E. E. Kadel, H. Koeppen, J. L. Astarita, R. Cubas, S. Jhunjhunwala, R. Banchereau, Y. Yang, Y. Guan, C. Chalouni, J. Ziai, Y. Şenbabaoğlu, S. Santoro, D. Sheinson, J. Hung, J. M. Giltnane, A. A. Pierce, K. Mesh, S. Lianoglou, J. Riegler, R. A. D. Carano, P. Eriksson, M. Höglund, L. Somarriba, D. L. Halligan, M. S. van der Heijden, Y. Loriot, J. E. Rosenberg, L. Fong, I. Mellman, D. S. Chen, M. Green, C. Derleth, G. D. Fine, P. S. Hegde, R. Bourgon, T. Powles, TGFβ attenuates tumour response to PD-L1 blockade by contributing to exclusion of T cells., *Nature* **554**, 544–548 (2018).

44. E. M. Van Allen, D. Miao, B. Schilling, S. A. Shukla, C. Blank, L. Zimmer, A. Sucker, U. Hillen, M. H. G. Foppen, S. M. Goldinger, J. Utikal, J. C. Hassel, B. Weide, K. C. Kaehler, C. Loquai, P. Mohr, R. Gutzmer, R. Dummer, S. Gabriel, C. J. Wu, D. Schadendorf, L. A. Garraway, Genomic correlates of response to CTLA-4 blockade in metastatic melanoma., *Science* **350**, 207–211 (2015).

45. T. N. Gide, C. Quek, A. M. Menzies, A. T. Tasker, P. Shang, J. Holst, J. Madore, S. Y. Lim, R. Velickovic, M. Wongchenko, Y. Yan, S. Lo, M. S. Carlino, A. Guminski, R. P. M. Saw, A. Pang, H. M. McGuire, U. Palendira, J. F. Thompson, H. Rizos, I. P. da Silva, M. Batten, R. A. Scolyer, G. V. Long, J. S. Wilmott, Distinct Immune Cell Populations Define Response to Anti-PD-1 Monotherapy and Anti-PD-1/Anti-CTLA-4 Combined Therapy., *Cancer Cell* **35**, 238–255.e6 (2019).

46. K. A. Schalper, M. E. Rodriguez-Ruiz, R. Diez-Valle, A. López-Janeiro, A. Porciuncula, M. A. Idoate, S. Inogés, C. de Andrea, A. López-Diaz de Cerio, S. Tejada, P. Berraondo, F. Villarroel-Espindola, J. Choi, A. Gúrpide, M. Giraldez, I. Goicoechea, J. Gallego Perez-Larraya, M. F. Sanmamed, J. L. Perez-Gracia, I. Melero, Neoadjuvant nivolumab modifies the tumor immune microenvironment in resectable glioblastoma., *Nat. Med.* **25**, 470–476 (2019).

47. A. C. Huang, R. J. Orlowski, X. Xu, R. Mick, S. M. George, P. K. Yan, S. Manne, A. A. Kraya, B. Wubbenhorst, L. Dorfman, K. D'Andrea, B. M. Wenz, S. Liu, L. Chilukuri, A. Kozlov, M. Carberry, L. Giles, M. W. Kier, F. Quagliarello, S. McGettigan, K. Kreider, L. Annamalai, Q. Zhao, R. Mogg, W. Xu, W. M. Blumenschein, J. H. Yearley, G. P. Linette, R. K. Amaravadi, L. M. Schuchter, R. S. Herati, B. Bengsch, K. L. Nathanson, M. D. Farwell, G. C. Karakousis, E. J. Wherry, T. C. Mitchell, A single dose of neoadjuvant PD-1 blockade predicts clinical outcomes in resectable melanoma., *Nat. Med.* **25**, 454–461 (2019).

48. M. Sade-Feldman, K. Yizhak, S. L. Bjorgaard, J. P. Ray, C. G. de Boer, R. W. Jenkins, D. J. Lieb, J. H. Chen, D. T. Frederick, M. Barzily-Rokni, S. S. Freeman, A. Reuben, P. J. Hoover, A.-C. Villani, E. Ivanova, A. Portell, P. H. Lizotte, A. R. Aref, J.-P. Eliane, M. R. Hammond, H. Vitzthum, S. M. Blackmon, B. Li, V. Gopalakrishnan, S. M. Reddy, Z. A. Cooper, C. P. Paweletz, D. A. Barbie, A. Stemmer-Rachamimov, K. T. Flaherty, J. A. Wargo, G. M. Boland, R. J. Sullivan,

G. Getz, N. Hacohen, Defining T Cell States Associated with Response to Checkpoint Immunotherapy in Melanoma., *Cell* **175**, 998–1013.e20 (2018).

49. A. H. Lee, L. Sun, A. Y. Mochizuki, J. G. Reynoso, J. Orpilla, F. Chow, J. C. Kienzler, R. G. Everson, D. A. Nathanson, S. J. Bensinger, L. M. Liau, T. Cloughesy, W. Hugo, R. M. Prins, Neoadjuvant PD-1 blockade induces T cell and cDC1 activation but fails to overcome the immunosuppressive tumor associated macrophages in recurrent glioblastoma., *Nat. Commun.* **12**, 6938 (2021).

50. J. Sprooten, J. Ceusters, A. Coosemans, P. Agostinis, S. De Vleeschouwer, L. Zitvogel, G. Kroemer, L. Galluzzi, A. D. Garg, Trial watch: dendritic cell vaccination for cancer immunotherapy., *Oncoimmunology* **8**, e1638212 (2019).

51. D. K. Irvin, E. Jouanneau, G. Duvall, X.-X. Zhang, Y. Zhai, D. Sarayba, A. Seksenyan, A. Panwar, K. L. Black, C. J. Wheeler, T cells enhance stem-like properties and conditional malignancy in gliomas., *PLoS One* **5**, e10974 (2010).

52. T. F. Cloughesy, A. Y. Mochizuki, J. R. Orpilla, W. Hugo, A. H. Lee, T. B. Davidson, A. C. Wang, B. M. Ellingson, J. A. Rytlewski, C. M. Sanders, E. S. Kawaguchi, L. Du, G. Li, W. H. Yong, S. C. Gaffey, A. L. Cohen, I. K. Mellinghoff, E. Q. Lee, D. A. Reardon, B. J. O'Brien, N. A. Butowski, P. L. Nghiemphu, J. L. Clarke, I. C. Arrillaga-Romany, H. Colman, T. J. Kaley, J. F. de Groot, L. M. Liau, P. Y. Wen, R. M. Prins, Neoadjuvant anti-PD-1 immunotherapy promotes a survival benefit with intratumoral and systemic immune responses in recurrent glioblastoma., *Nat. Med.* **25**, 477–486 (2019).

53. M. Rapp, O. M. Grauer, M. Kamp, N. Sevens, N. Zotz, M. Sabel, R. V. Sorg, A randomized controlled phase II trial of vaccination with lysate-loaded, mature dendritic cells integrated into standard radiochemotherapy of newly diagnosed glioblastoma (GlioVax): study protocol for a randomized controlled trial., *Trials* **19**, 293 (2018).

54. V. van der Heide, E. Humblin, A. Vaidya, A. O. Kamphorst, Advancing beyond the twists and turns of T cell exhaustion in cancer., *Sci. Transl. Med.* **14**, eabo4997 (2022).

55. T. Le, T. Phan, M. Pham, D. Tran, L. Lam, T. Nguyen, T. Truong, H. Vuong, T. Luu, N. Phung, T. Nguyen, O. Pham, A. Nguyen, H. Nguyen, H. Tran, L. Tran, H. A. Nguyen, T. Tran, N. Nguyen, N. Tran, C. Boysen, U. Nguyen, V. Pham, K. Theodore, N. Pham, T. Gill, S. Pham, BBrowser: Making single-cell data easily accessible, *BioRxiv* (2020), doi:10.1101/2020.12.11.414136.

56. M. J. Goldman, B. Craft, M. Hastie, K. Repečka, F. McDade, A. Kamath, A. Banerjee, Y. Luo, D. Rogers, A. N. Brooks, J. Zhu, D. Haussler, Visualizing and interpreting cancer genomics data via the Xena platform., *Nat. Biotechnol.* **38**, 675–678 (2020).

57. M. Deng, J. Brägelmann, I. Kryukov, N. Saraiva-Agostinho, S. Perner, FirebrowseR: an R client to the Broad Institute's Firehose Pipeline., *Database (Oxford)* **2017** (2017), doi:10.1093/database/baw160.

58. P. Charoentong, F. Finotello, M. Angelova, C. Mayer, M. Efremova, D. Rieder, H. Hackl, Z. Trajanoski, Pan-cancer Immunogenomic Analyses Reveal Genotype-Immunophenotype Relationships and Predictors of Response to Checkpoint Blockade., *Cell Rep.* **18**, 248–262 (2017).

59. T. Li, J. Fan, B. Wang, N. Traugh, Q. Chen, J. S. Liu, B. Li, X. S. Liu, TIMER: A Web Server for Comprehensive Analysis of Tumor-Infiltrating Immune Cells., *Cancer Res.* **77**, e108–e110 (2017).

60. S. Seabold, J. Perktold, Statsmodels: Econometric and statistical modeling with python, *PROC. OF THE 9th PYTHON IN SCIENCE CONF. (SCIPY 2010)* **http://conference.scipy.org/proceedings/scipy2010/pdfs/seabold.pdf** (2010) (available at https://pdfs.semanticscholar.org/3a27/6417e5350e29cb6bf04ea5a4785601d5a215.pdf).

61. A. M. Newman, C. L. Liu, M. R. Green, A. J. Gentles, W. Feng, Y. Xu, C. D. Hoang, M. Diehn, A. A. Alizadeh, Robust enumeration of cell subsets from tissue expression profiles., *Nat. Methods* **12**, 453–457 (2015).

62. M. Waskom, seaborn: statistical data visualization*Seaborn* (2020).

63. F. A. Wolf, P. Angerer, F. J. Theis, SCANPY: large-scale single-cell gene expression data analysis, *Genome Biol.* **19**, 15 (2018).

64. G. Sturm, T. Szabo, G. Fotakis, M. Haider, D. Rieder, Z. Trajanoski, F. Finotello, Scirpy: a Scanpy extension for analyzing single-cell T-cell receptor-sequencing data., *Bioinformatics* **36**, 4817–4818 (2020).

65. A. Behdenna, J. Haziza, C.-A. Azencott, A. Nordor, pyComBat, a Python tool for batch effects correction in high-throughput molecular data using empirical Bayes methods, *BioRxiv* (2020), doi:10.1101/2020.03.17.995431.

66. D. Sun, J. Wang, Y. Han, X. Dong, J. Ge, R. Zheng, X. Shi, B. Wang, Z. Li, P. Ren, L. Sun, Y. Yan, P. Zhang, F. Zhang, T. Li, C. Wang, TISCH: a comprehensive web resource enabling interactive single-cell transcriptome visualization of tumor microenvironment., *Nucleic Acids Res.* **49**, D1420–D1430 (2021).

67. E. Becht, L. McInnes, J. Healy, C.-A. Dutertre, I. W. H. Kwok, L. G. Ng, F. Ginhoux, E. W. Newell, Dimensionality reduction for visualizing single-cell data using UMAP., *Nat. Biotechnol.* **37**, 38–44 (2018).

68. F. A. Wolf, F. K. Hamey, M. Plass, J. Solana, J. S. Dahlin, B. Göttgens, N. Rajewsky, L. Simon, F. J. Theis, PAGA: graph abstraction reconciles clustering with trajectory inference through a topology preserving map of single cells., *Genome Biol.* **20**, 59 (2019).

69. V. A. Traag, L. Waltman, N. J. van Eck, From Louvain to Leiden: guaranteeing well-connected communities., *Sci. Rep.* **9**, 5233 (2019).

70. *Ährenlese - ausgewählte Aufsätze und ein Vortrag* (Erich A. Hausmann, Zürich, 1999).

71. P. Shannon, A. Markiel, O. Ozier, N. S. Baliga, J. T. Wang, D. Ramage, N. Amin, B. Schwikowski, T. Ideker, Cytoscape: a software environment for integrated models of biomolecular interaction networks., *Genome Res.* **13**, 2498–2504 (2003).

72. H. Zola, B. Swart, I. Nicholson, E. Voss, *Leukocyte and stromal cell molecules: the CD markers* (books.google.com, 2007).

73. M. D. Martin, V. P. Badovinac, Defining memory CD8 T cell., *Front. Immunol.* **9**, 2692 (2018).

74. D. Herndler-Brandstetter, H. Ishigame, R. Shinnakasu, V. Plajer, C. Stecher, J. Zhao, M. Lietzenmayer, L. Kroehling, A. Takumi, K. Kometani, T. Inoue, Y. Kluger, S. M. Kaech, T. Kurosaki, T. Okada, R. A. Flavell, KLRG1+ Effector CD8+ T Cells Lose KLRG1, Differentiate

into All Memory T Cell Lineages, and Convey Enhanced Protective Immunity., *Immunity* **48**, 716–729.e8 (2018).

75. M. St Paul, P. S. Ohashi, The roles of CD8+ T cell subsets in antitumor immunity., *Trends Cell Biol.* **30**, 695–704 (2020).

76. M. Efremova, M. Vento-Tormo, S. A. Teichmann, R. Vento-Tormo, CellPhoneDB: inferring cell-cell communication from combined expression of multi-subunit ligand-receptor complexes., *Nat. Protoc.* **15**, 1484–1506 (2020).

77. Y. Liao, J. Wang, E. J. Jaehnig, Z. Shi, B. Zhang, WebGestalt 2019: gene set analysis toolkit with revamped UIs and APIs., *Nucleic Acids Res.* **47**, W199–W205 (2019).

78. G. Parisi, J. D. Saco, F. B. Salazar, J. Tsoi, P. Krystofinski, C. Puig-Saus, R. Zhang, J. Zhou, G. C. Cheung-Lau, A. J. Garcia, C. S. Grasso, R. Tavaré, S. Hu-Lieskovan, S. Mackay, J. Zalevsky, C. Bernatchez, A. Diab, A. M. Wu, B. Comin-Anduix, D. Charych, A. Ribas, Persistence of adoptively transferred T cells with a kinetically engineered IL-2 receptor agonist., *Nat. Commun.* **11**, 660 (2020).

79. M. L. Axelrod, M. J. Nixon, P. I. Gonzalez-Ericsson, R. E. Bergman, M. A. Pilkinton, W. J. McDonnell, V. Sanchez, S. R. Opalenik, S. Loi, J. Zhou, S. Mackay, B. N. Rexer, V. G. Abramson, V. M. Jansen, S. Mallal, J. Donaldson, S. M. Tolaney, I. E. Krop, A. C. Garrido-Castro, J. D. Marotti, K. Shee, T. W. Miller, M. E. Sanders, I. A. Mayer, R. Salgado, J. M. Balko, Changes in Peripheral and Local Tumor Immunity after Neoadjuvant Chemotherapy Reshape Clinical Outcomes in Patients with Breast Cancer., *Clin. Cancer Res.* **26**, 5668–5681 (2020).

80. C. Ma, A. F. Cheung, T. Chodon, R. C. Koya, Z. Wu, C. Ng, E. Avramis, A. J. Cochran, O. N. Witte, D. Baltimore, B. Chmielowski, J. S. Economou, B. Comin-Anduix, A. Ribas, J. R. Heath, Multifunctional T-cell analyses to study response and progression in adoptive cell transfer immunotherapy., *Cancer Discov.* **3**, 418–429 (2013).

81. J. Huang, J. Zhou, R. Ghinnagow, T. Seki, S. Iketani, D. Soulard, P. Paczkowski, Y. Tsuji, S. MacKay, L. J. Cruz, F. Trottein, M. Tsuji, Targeted Co-delivery of Tumor Antigen and α-Galactosylceramide to CD141+ Dendritic Cells Induces a Potent Tumor Antigen-Specific Human CD8+ T Cell Response in Human Immune System Mice., *Front. Immunol.* **11**, 2043 (2020).

82. M. Setty, V. Kiseliovas, J. Levine, A. Gayoso, L. Mazutis, D. Pe'er, Characterization of cell fate probabilities in single-cell data with Palantir., *Nat. Biotechnol.* **37**, 451–460 (2019).

83. J. Rossi, P. Paczkowski, Y.-W. Shen, K. Morse, B. Flynn, A. Kaiser, C. Ng, K. Gallatin, T. Cain, R. Fan, S. Mackay, J. R. Heath, S. A. Rosenberg, J. N. Kochenderfer, J. Zhou, A. Bot, Preinfusion polyfunctional anti-CD19 chimeric antigen receptor T cells are associated with clinical outcomes in NHL., *Blood* **132**, 804–814 (2018).

84. A. R. Pombo Antunes, I. Scheyltjens, F. Lodi, J. Messiaen, A. Antoranz, J. Duerinck, D. Kancheva, L. Martens, K. De Vlaminck, H. Van Hove, S. S. Kjølner Hansen, F. M. Bosisio, K. Van der Borght, S. De Vleeschouwer, R. Sciot, L. Bouwens, M. Verfaillie, N. Vandamme, R. E. Vandenbroucke, O. De Wever, Y. Saeys, M. Guilliams, C. Gysemans, B. Neyns, F. De Smet, D. Lambrechts, J. A. Van Ginderachter, K. Movahedi, Single-cell profiling of myeloid cells in glioblastoma across species and disease stage reveals macrophage competition and specialization., *Nat. Neurosci.* **24**, 595–610 (2021).

85. G. Pau, F. Fuchs, O. Sklyar, M. Boutros, W. Huber, EBImage--an R package for image processing with applications to cellular phenotypes., *Bioinformatics* **26**, 979–981 (2010).

86. J. C. Caicedo, S. Cooper, F. Heigwer, S. Warchal, P. Qiu, C. Molnar, A. S. Vasilevich, J. D. Barry, H. S. Bansal, O. Kraus, M. Wawer, L. Paavolainen, M. D. Herrmann, M. Rohban, J. Hung, H. Hennig, J. Concannon, I. Smith, P. A. Clemons, S. Singh, P. Rees, P. Horvath, R. G. Linington, A. E. Carpenter, Data-analysis strategies for image-based cell profiling., *Nat. Methods* **14**, 849–863 (2017).

87. J. H. Levine, E. F. Simonds, S. C. Bendall, K. L. Davis, E. D. Amir, M. D. Tadmor, O. Litvin, H. G. Fienberg, A. Jager, E. R. Zunder, R. Finck, A. L. Gedman, I. Radtke, J. R. Downing, D. Pe'er, G. P. Nolan, Data-Driven Phenotypic Dissection of AML Reveals Progenitor-like Cells that Correlate with Prognosis., *Cell* **162**, 184–197 (2015).

88. S. Van Gassen, B. Callebaut, M. J. Van Helden, B. N. Lambrecht, P. Demeester, T. Dhaene, Y. Saeys, FlowSOM: Using self-organizing maps for visualization and interpretation of cytometry data., *Cytometry A* **87**, 636–645 (2015).

89. J. Fu, K. Li, W. Zhang, C. Wan, J. Zhang, P. Jiang, X. S. Liu, Large-scale public data reuse to model immunotherapy response and resistance., *Genome Med.* **12**, 21 (2020).

90. D. Szklarczyk, A. Franceschini, S. Wyder, K. Forslund, D. Heller, J. Huerta-Cepas, M. Simonovic, A. Roth, A. Santos, K. P. Tsafou, M. Kuhn, P. Bork, L. J. Jensen, C. von Mering, STRING v10: protein-protein interaction networks, integrated over the tree of life., *Nucleic Acids Res.* **43**, D447–52 (2015).

**ACKNOWLEDGEMENTS:** We acknowledge Alexander Huang and Tara Mitchell (University of Pennsylvania) for helping us in accessing the patient survival data from their SKCM clinical trial. We thank N Van Baren and P Coulie (De Duve Institute), as well as Y Hua (KU Leuven-VIB), for reading the manuscript and providing valuable feedback.

**FUNDING**: This study is supported by Research Foundation Flanders (FWO) (Fundamental Research Grant, G0B4620N to ADG; Excellence of Science/EOS grant, 30837538, for 'DECODE' consortium, for ADG, BJVDE), KU Leuven (C1 grant, C14/19/098; C3 grant, C3/21/037; and POR award funds, POR/16/040 to ADG), Kom op Tegen Kanker (KOTK/2018/11509/1 to SDV, ADG, FDS; and KOTK/2019/11955/1 to ADG) and VLIR-UOS (iBOF grant, iBOF/21/048, for 'MIMICRY' consortium to ADG and ST). IV is supported by FWO-SB PhD Fellowship (1S06821N). JS is funded by Kom op tegen Kanker (Stand up to Cancer), the Flemish cancer society through the Emmanuel van der Schueren (EvDS) PhD fellowship (projectID: 12699). DMB got support from Senior Postdoctoral FWO fellowship (1279223N), KU Leuven's Postdoctoral mandate grant (PDMT1/21/032), and the Belgian Federation against Cancer grant numbers 2018-127 and 2016-133 as well as a grant from Fondation Roi-Baudouin to ST. RSL is supported by FWO-SB PhD Fellowship (1S44123N). ST is further supported by a Senior Clinical Investigator award of FWO. AD, MCS and RVS were supported by a grant from the Federal Ministry of Education and Research (BMBF; grant #01KG1242). DL is supported by FWO Medium-scale infrastructure grant (I001818N) and FWO research project (G093821N). This work is also supported by KU Leuven grant C14/17/084 to FDS and C3/19/053 to FDS and FMB, FWO grant G0I1118N to FDS, the Leuven Kankerinstituut (LKI), and an FWO fellowship to JM (1156520N). AMA is supported by the Opening the Future Foundation and LKI.

**AUTHOR CONTRIBUTIONS:** SN was the lead researcher and performed most of the multi-omics bioinformatics analyses, coordinated & managed the research efforts, and created the figures. DMB helped closely with single-cell bioinformatics and critical discussion on biostatistics. AAM, JM, YVH, FB, and FDS executed the MILAN analyses. JS, JG, RSL and IV

helped with the manuscript, experimental work, and figure preparation. AD, MCS, MR and RVS collected relevant patient samples, performed immunophenotyping and data analyses from the GlioVax clinical trial. DP, MD, and FDS executed the sample collection and initial patient sample preparation for single cell secretome. WN and SM executed the single cell secretome analyses. LG executed the mathematical modelling of cell cycle. OB, MV, and SDV helped with patient sample collection. DL, TV, SM, GB, AL, BJVDE, ST, and JB helped with critical data interpretation, provided expert conceptual or data-analyses views, or helped with manuscript writing. ADG, FDS, RVS, and FB provided supervision for the research, participated in data analyses and decision-making, and revised the manuscript. ADG was the lead investigator of the project and coordinated the overall project, supervised the research design, and wrote the manuscript.

**COMPETING INTERESTS:** ADG received consulting/advisory/lecture honoraria from Boehringer Ingelheim, Novigenix, Isoplexis and Miltenyi Biotec. WN and SM are employed by and have equity ownership in IsoPlexis (USA). BVDE has equity or stock options holding of iTeos Therapeutics and Oncorus and performed paid advisory consulting (SAB member) for Amgen, iTeos Therapeutics, Oncorus, Esobiotec, and Vaccitech. GB is scientific co-founder of Oncurious.

**DATA & MATERIALS AVAILABILITY:** All data associated with this study are in the paper or supplementary materials. TCGA data are publicly available from Xena - http://xena.ucsc.edu, FireBrowse portal (a Broad Institute GDAC Firehose analyses pipeline: http://firebrowse.org/), or TCGA PanCancerAtlas Immune Response Working Group's Cancer Research Institute (CRI) iAtlas Explorer (https://gdc.cancer.gov/about-data/publications/panimmune). Single-cell data integrated in this study (scRNA-seq, scTCR-seq and CyTOF) can be accessed from the following public resources: TISCH database (http://tisch.comp-genomics.org/), GEO database (GSE123139, GSE157829, GSE149652, GSE114724, GSE163108, GSE179994, GSM4455935, GSM6474823, GSE159251), BROAD single-cell analysis data portal (SCP393,

SCP11), https://lambrechtslab.sites.vib.be/en/data-access, or FlowRepository (FR-FCM-Z2B3). IEDB immuno-peptidome assay data is available through https://www.iedb.org. GBM anatomical-zone based spatial transcriptomics data was accessed from the IVY-GAP data portal (https://glioblastoma.alleninstitute.org/). Cross-sectional tumor transcriptomic data from clinical trials were accessed using a standardized TIDE data-portal (http://tide.dfci.harvard.edu/login/) or Cancer Research Institute (CRI) iAtlas Explorer (https://www.cri-iatlas.org/). Data from longitudinal clinical trials involving resectable-SKCM or resectable-GBM treated with neoadjuvant anti-PD-1 immunotherapy were accessed from referenced published sources or requested from the original investigators. DC vaccination data were accessed here from the GEO database (GSE11100). All computational methods, code, equations, and source data (Isoplexis single cell secretome data, amongst others) wherever applicable are described in the supplemental materials and methods section or available on Synapse, a Sage Bionetworks repository (syn40323295) (e.g., scripts to reproduce our analyses). The scRNA-seq and scTCR-seq dataset and the multi-cancer meta-data of the T cell-activating immunopeptidome are available on Synapse (syn40323295). Raw data and genetic signatures associated with various computational outputs are described in **data files S1** to **S6**. Data and materials relevant for MILAN analyses are available from Frederik De Smet upon reasonable request and subject to a material transfer agreement (MTA). Original datasets created for this study, based on public datasets, and associated data for which the license permits, are available on Synapse (syn40323295). The full list of library versions used is available in **data file S6**.

## MAIN FIGURE LEGENDS

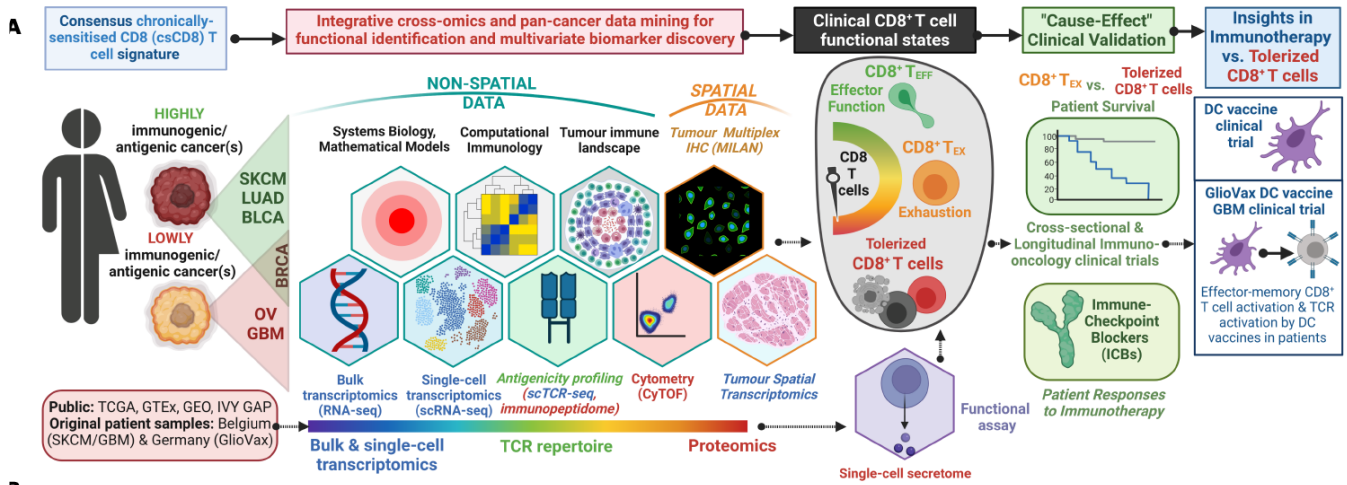
A
Consensus chronically-sensitised CD8 (csCD8) T cell signature
Integrative cross-omics and pan-cancer data mining for functional identification and multivariate biomarker discovery
Clinical CD8+ T cell functional states
"Cause-Effect" Clinical Validation
Insights in Immunotherapy vs. Tolerized CD8+ T cells
NON-SPATIAL DATA
SPATIAL DATA
Systems Biology, Mathematical Models
Computational Immunology
Tumour immune landscape
Tumour Multiplex IHC (MILAN)
HIGHLY immunogenic/ antigenic cancer(s)
LOWLY immunogenic/ antigenic cancer(s)
SKCM
LUAD
BLCA
BRCA
OV
GBM
Public: TCGA, GTEx, GEO, IVY GAP
Original patient samples: Belgium (SKCM/GBM) & Germany (GlioVax)
Bulk transcriptomics (RNA-seq)
Single-cell transcriptomics (scRNA-seq)
Antigenicity profiling (scTCR-seq, immunopeptidome)
Cytometry (CyTOF)
Tumour Spatial Transcriptomics
Bulk & single-cell transcriptomics
TCR repertoire
Proteomics
Single-cell secretome
Functional assay
CD8+ TEFF
Effector Function
CD8 T cells
CD8+ TEX
Exhaustion
Tolerized CD8+ T cells
CD8+ TEX vs. Tolerized CD8+ T cells
Patient Survival
Cross-sectional & Longitudinal Immuno-oncology clinical trials
Immune-Checkpoint Blockers (ICBs)
Patient Responses to Immunotherapy
DC vaccine clinical trial
GlioVax DC vaccine GBM clinical trial
Effector-memory CD8+ T cell activation & TCR activation by DC vaccines in patients

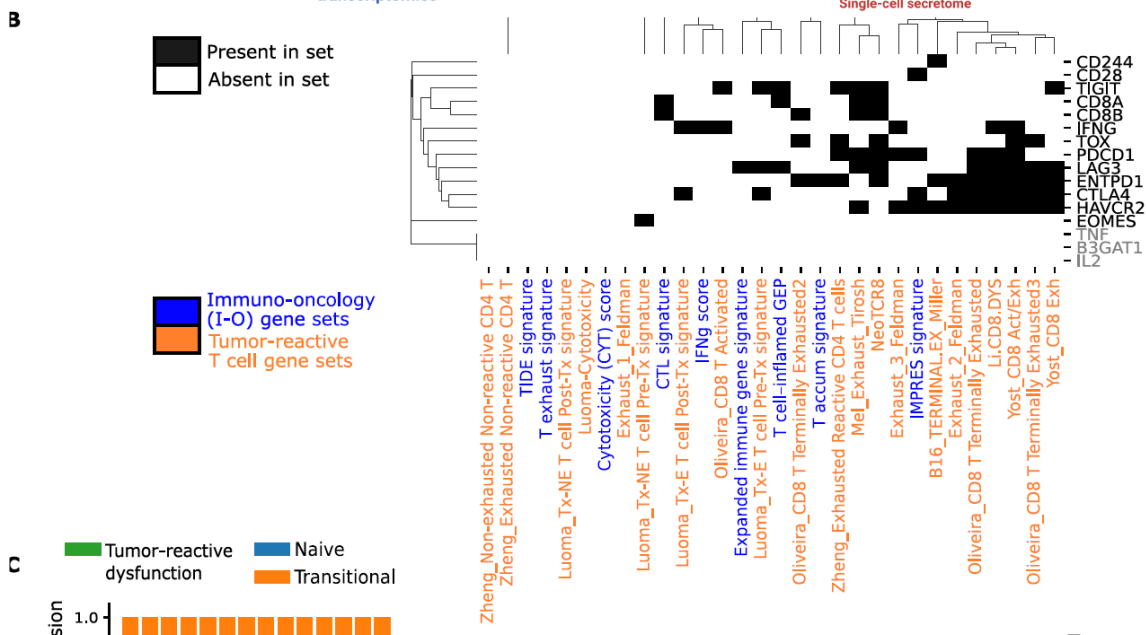
B
Present in set
Absent in set
CD244
CD28
TIGIT
CD8A
CD8B
IFNG
TOX
PDCD1
LAG3
ENTPD1
CTLA4
HAVCR2
EOMES
TNF
B3GAT1
IL2
Immuno-oncology (I-O) gene sets
Tumor-reactive T cell gene sets
Zheng_Non-exhausted Non-reactive CD4 T
Zheng_Exhausted Non-reactive CD4 T
TIDE signature
T exhaust signature
Luoma_Tx-NE T cell Post-Tx signature
Luoma-Cytotoxicity
Cytotoxicity (CYT) score
Exhaust_1_Feldman
Luoma_Tx-NE T cell Pre-Tx signature
CTL signature
Luoma_Tx-E T cell Post-Tx signature
IFNg score
Oliveira_CD8 T Activated
Expanded immune gene signature
Luoma_Tx-E T cell Pre-Tx signature
T cell-inflamed GEP
Oliveira_CD8 T Terminally Exhausted2
T accum signature
Zheng_Exhausted Reactive CD4 T cells
Mel_Exhaust_Tirosh
NeoTCR8
Exhaust_3_Feldman
IMPRES signature
B16_TERMINAL.EX_Miller
Exhaust_2_Feldman
Oliveira_CD8 T Terminally Exhausted
Li.CD8.DYS
Yost_CD8 Act/Exh
Oliveira_CD8 T Terminally Exhausted3
Yost_CD8 Exh

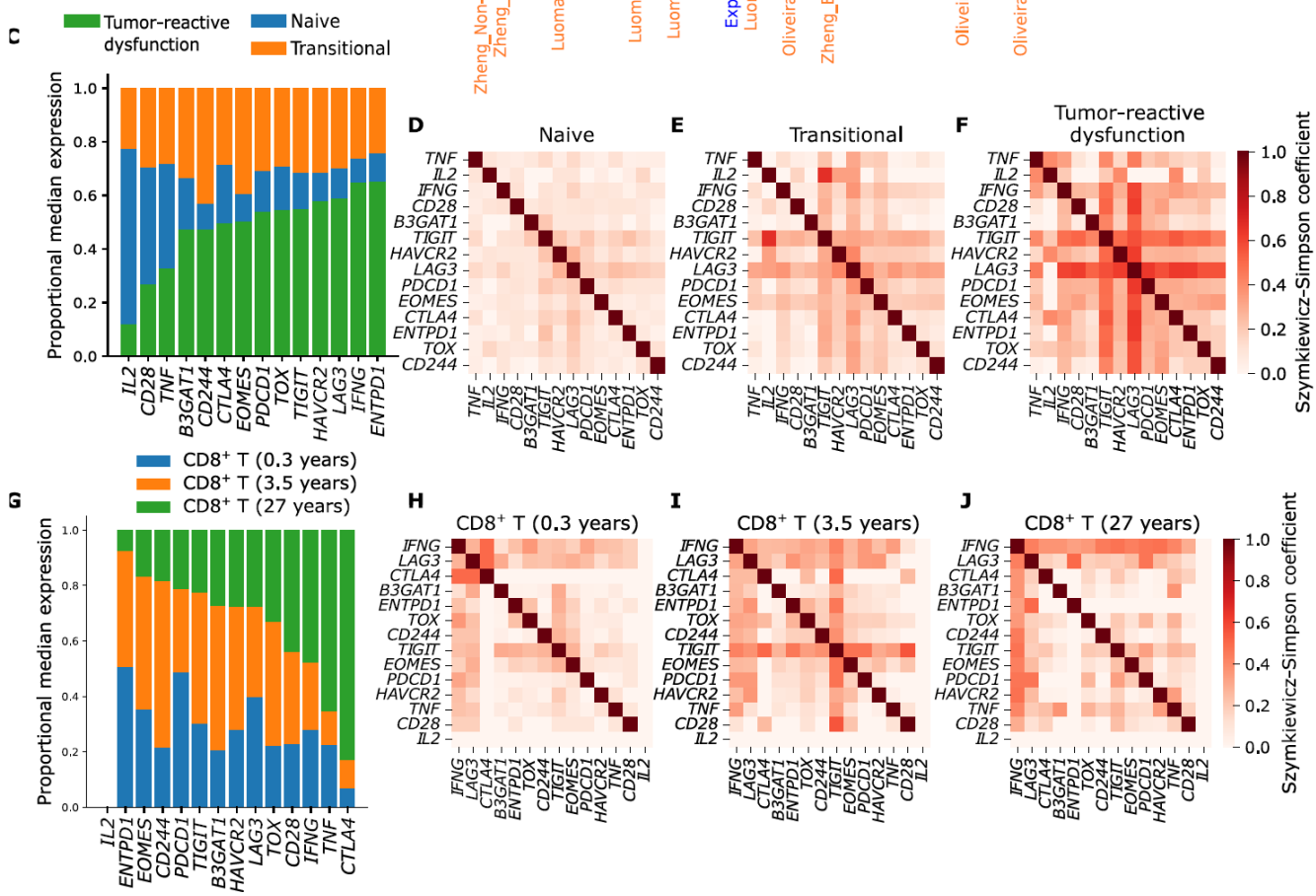
C
Tumor-reactive dysfunction
Naive
Transitional
Proportional median expression
IL2
CD28
TNF
B3GAT1
CD244
CTLA4
EOMES
PDCD1
TOX
TIGIT
HAVCR2
LAG3
IFNG
ENTPD1
D
Naive
E
Transitional
F
Tumor-reactive dysfunction
Szymkiewicz-Simpson coefficient
G
CD8+ T (0.3 years)
CD8+ T (3.5 years)
CD8+ T (27 years)
Proportional median expression
IL2
ENTPD1
EOMES
CD244
PDCD1
TIGIT
B3GAT1
HAVCR2
LAG3
TOX
CD28
IFNG
TNF
CTLA4
H
CD8+ T (0.3 years)
I
CD8+ T (3.5 years)
J
CD8+ T (27 years)
Szymkiewicz-Simpson coefficient

**Figure 1. Signature-based immunogenomics were used to characterize the CD8$^+$ T cell landscape. (A)** Schematics of our study design to differentiate tumor-reactivity induced exhaustion (CD8$^+$ $T_{EX}$) from other hypofunctional CD8$^+$ T cell states. The analysis spanned both publicly available and in-house patient cohorts, with non-spatial (bulk and single-cell transcriptomics, scTCR-seq, and immuno-peptidomics) and spatial (multiplexed protein, transcriptomic) analysis. These results were validated with functional profiling and with clinical trial data. **(B)** Shown is a comparison of the most used signatures to describe T cell exhaustion. We collected 21 published tumor-reactive T cell-associated genetic signatures (marked in orange) and clinical trial-relevant signatures and performed gene overlap analyses with the csCD8$^+$ T cell signature. **(C to J)** Stacked bar-plots based on median gene expression **(C, G)** and correlation matrices **(D, E, F, H, I, J)** are shown for the following: genes from csCD8$^+$ T cell signature for which expression was reported in a melanoma scRNA-seq cohort, covering CD8$^+$ T cells with naïve (**C**, **D**, 5378 cells), transitional (**C**, **E**, 4189 cells) or tumor-reactive dysfunctional phenotypes (**C**, **F**, 10120 cells); or single-cell CD8$^+$ T cell profiles from individuals infected with HIV for 0.3 years (**G**, **H**, 1596 cells), 3.5 years (**G**, **I**, 841 cells) or 27 years (**G**, **J**, 1304 cells).

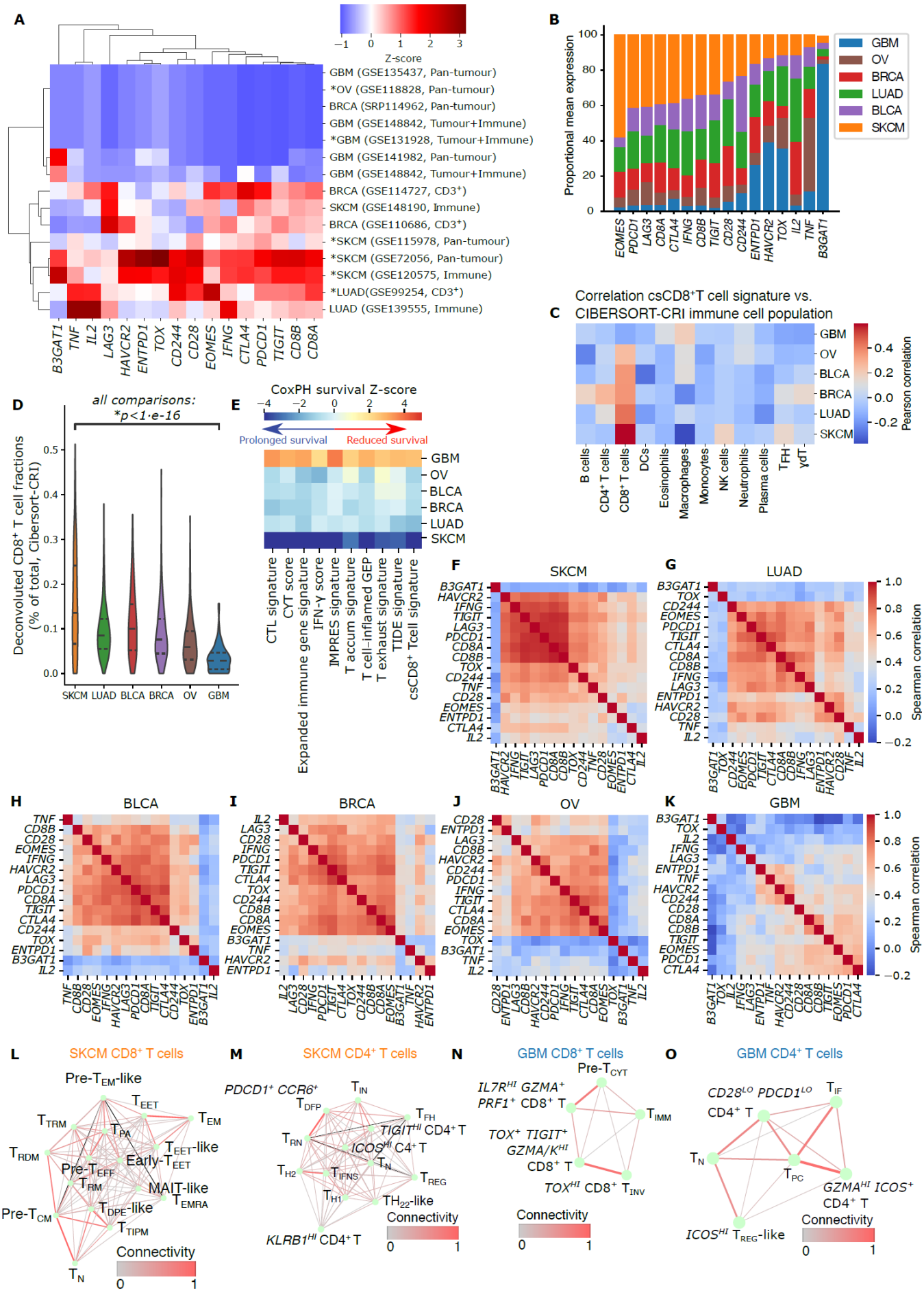
A
Z-score
GBM (GSE135437, Pan-tumour)
*OV (GSE118828, Pan-tumour)
BRCA (SRP114962, Pan-tumour)
GBM (GSE148842, Tumour+Immune)
*GBM (GSE131928, Tumour+Immune)
GBM (GSE141982, Pan-tumour)
GBM (GSE148842, Tumour+Immune)
BRCA (GSE114727, CD3+)
SKCM (GSE148190, Immune)
BRCA (GSE110686, CD3+)
*SKCM (GSE115978, Pan-tumour)
*SKCM (GSE72056, Pan-tumour)
*SKCM (GSE120575, Immune)
*LUAD(GSE99254, CD3+)
LUAD (GSE139555, Immune)
B3GAT1 TNF IL2 LAG3 HAVCR2 ENTPD1 TOX CD244 CD28 EOMES IFNG CTLA4 PDCD1 TIGIT CD8B CD8A
B
Proportional mean expression
GBM
OV
BRCA
LUAD
BLCA
SKCM
EOMES PDCD1 LAG3 CD8A CTLA4 IFNG CD8B TIGIT CD28 CD244 ENTPD1 HAVCR2 TOX IL2 TNF B3GAT1
C
Correlation csCD8+T cell signature vs.
CIBERSORT-CRI immune cell population
Pearson correlation
B cells
CD4+ T cells
CD8+ T cells
DCs
Eosinophils
Macrophages
Monocytes
NK cells
Neutrophils
Plasma cells
TFH
γdT
D
all comparisons:
*p<1·e-16
Deconvoluted CD8+ T cell fractions
(% of total, Cibersort-CRI)
SKCM LUAD BLCA BRCA OV GBM
E
CoxPH survival Z-score
Prolonged survival
Reduced survival
CTL signature
CYT score
Expanded immune gene signature
IFN-γ score
IMPRES signature
T accum signature
T cell-inflamed GEP
T exhaust signature
TIDE signature
csCD8+ Tcell signature
F
SKCM
G
LUAD
Spearman correlation
H
BLCA
I
BRCA
J
OV
K
GBM
L
SKCM CD8+ T cells
Pre-TEM-like
TEET
TEM
TTRM
TPA
TRDM
TEET-like
Early-TEET
Pre-TEFF
TRM
MAIT-like
TEMRA
Pre-TCM
TDPE-like
TTIPM
TN
Connectivity
M
SKCM CD4+ T cells
PDCD1+ CCR6+
TIN
TDFP
TFH
TIGIT^HI CD4+ T
TRN
ICOS^HI C4+ T
TN
TH2
TIFNS
TREG
TH1
TH22-like
KLRB1^HI CD4+ T
N
GBM CD8+ T cells
Pre-TCYT
IL7R^HI GZMA+
PRF1+ CD8+ T
TIMM
TOX+ TIGIT+
GZMA/K^HI
CD8+ T
TOX^HI CD8+ TINV
O
GBM CD4+ T cells
CD28^LO PDCD1^LO
TIF
CD4+ T
TN
TPC
GZMA^HI ICOS+
CD4+ T
ICOS^HI TREG-like

**Figure 2. The CD8$^+$ T cell landscape differs between cancer types. (A)** Expression of the csCD8$^+$ T cell-signature genes in 15 scRNAseq studies covering 5 cancer types. Smart-seq2 data are marked with an asterisk. **(B)** Stacked bar-plot showing normalized mean expression of the 16 signature genes over six tumor-types (BLCA, n=426; BRCA, n=1212; GBM, n=171; LUAD, n=574; OV, n=427, SKCM, n=470). **(C)** Z-score column standardized Pearson's correlations between CIBERSORT-CRI inferred immune cell fractions and csCD8$^+$ T cell-signature expression per cancer type in TCGA. **(D)** Violin plots for CD8$^+$ T cell fractions (CIBERSORT-CRI). The violin plots show median and 25th-75th percentiles. Data were analyzed using the Kruskal-Wallis test. Pairwise comparisons were made using the Dunn posthoc test, using holm-sidak correction ($p < 0.05$ for significance, median and 25%-75% percentiles indicated within violins). **(E)** Patient-based CoxPH regression Z-scores (95% confidence interval) from TCGA, indicating prognostic value of various signatures (BLCA, n=406; BRCA, n=1090; GBM, n=159; LUAD, n=504; OV, n=420, SKCM, n=451). **(F to K**) Matrices show the Spearman correlation between the expression of the indicated genes from csCD8$^+$ T cell-signature for SKCM **(F)**, LUAD **(G)**, BLCA **(H)**, BRCA **(I)**, OV **(J)** or GBM **(K)**. **(L to O)** Partition-based graph abstraction (PAGA) derived T single-cell subpopulation connectivity networks are shown for SKCM-CD8$^+$ T cells **(L)**, SKCM-CD4$^+$ T cells **(M)**, GBM-CD8$^+$ T cells **(N)**, and GBM-CD4$^+$ T cells **(O)**. Please see **data file S2** for the full annotations and abbreviations for above sub-population nomenclatures **(L to O)**. Marker details are in fig. S4.

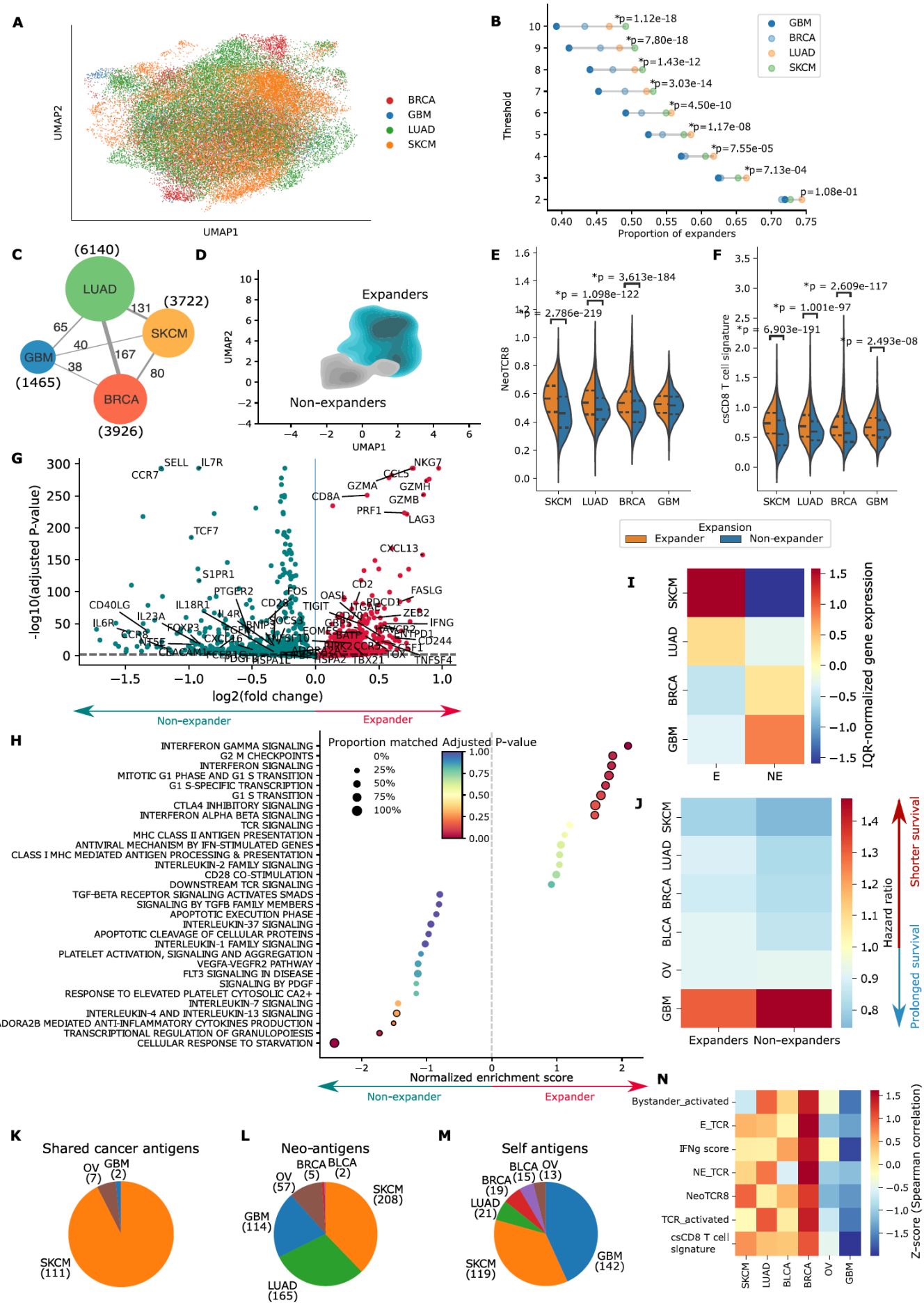
A
UMAP2
UMAP1
BRCA
GBM
LUAD
SKCM
B
Threshold
Proportion of expanders
*p=1.12e-18
*p=7.80e-18
*p=1.43e-12
*p=3.03e-14
*p=4.50e-10
*p=1.17e-08
*p=7.55e-05
*p=7.13e-04
p=1.08e-01
C
(6140)
(3722)
(1465)
(3926)
131
65
40
167
38
80
D
Expanders
Non-expanders
UMAP2
UMAP1
E
NeoTCR8
*p = 3.613e-184
*p = 1.098e-122
*p = 2.786e-219
F
csCD8 T cell signature
*p = 2.609e-117
*p = 1.001e-97
*p = 6.903e-191
*p = 2.493e-08
SKCM LUAD BRCA GBM
Expansion
Expander
Non-expander
G
-log10(adjusted P-value)
log2(fold change)
Non-expander
Expander
SELL
IL7R
CCR7
NKG7
CCL5
GZMA
GZMH
CD8A
GZMB
PRF1
LAG3
TCF7
CXCL13
S1PR1
PTGER2
FOS
CD2
OASL
FASLG
CD40LG
IL18R1
CD28
TIGIT
ITGAE
PDCD1
ZEB2
IL6R
IL23A
IL4R
GBP2
IFNG
FOXP3
CCR8
CXCL16
BATF
CD244
TNFSF4
TBX21
TOX
H
Proportion matched Adjusted P-value
0%
25%
50%
75%
100%
INTERFERON GAMMA SIGNALING
G2 M CHECKPOINTS
INTERFERON SIGNALING
MITOTIC G1 PHASE AND G1 S TRANSITION
G1 S-SPECIFIC TRANSCRIPTION
G1 S TRANSITION
CTLA4 INHIBITORY SIGNALING
INTERFERON ALPHA BETA SIGNALING
TCR SIGNALING
MHC CLASS II ANTIGEN PRESENTATION
ANTIVIRAL MECHANISM BY IFN-STIMULATED GENES
CLASS I MHC MEDIATED ANTIGEN PROCESSING & PRESENTATION
INTERLEUKIN-2 FAMILY SIGNALING
CD28 CO-STIMULATION
DOWNSTREAM TCR SIGNALING
TGF-BETA RECEPTOR SIGNALING ACTIVATES SMADS
SIGNALING BY TGFB FAMILY MEMBERS
APOPTOTIC EXECUTION PHASE
INTERLEUKIN-37 SIGNALING
APOPTOTIC CLEAVAGE OF CELLULAR PROTEINS
INTERLEUKIN-1 FAMILY SIGNALING
PLATELET ACTIVATION, SIGNALING AND AGGREGATION
VEGFA-VEGFR2 PATHWAY
FLT3 SIGNALING IN DISEASE
SIGNALING BY PDGF
RESPONSE TO ELEVATED PLATELET CYTOSOLIC CA2+
INTERLEUKIN-7 SIGNALING
INTERLEUKIN-4 AND INTERLEUKIN-13 SIGNALING
ADORA2B MEDIATED ANTI-INFLAMMATORY CYTOKINES PRODUCTION
TRANSCRIPTIONAL REGULATION OF GRANULOPOIESIS
CELLULAR RESPONSE TO STARVATION
Normalized enrichment score
Non-expander
Expander
I
IQR-normalized gene expression
SKCM
LUAD
BRCA
GBM
E
NE
J
Hazard ratio
Shorter survival
Prolonged survival
BLCA
OV
Expanders Non-expanders
N
Bystander_activated
E_TCR
IFNg score
NE_TCR
NeoTCR8
TCR_activated
csCD8 T cell signature
Z-score (Spearman correlation)
K
Shared cancer antigens
OV (7)
GBM (2)
SKCM (111)
L
Neo-antigens
BRCA (5)
BLCA (2)
OV (57)
SKCM (208)
GBM (114)
LUAD (165)
M
Self antigens
BLCA (15)
OV (13)
BRCA (19)
LUAD (21)
SKCM (119)
GBM (142)

**Figure 3. Analysis of single-cell transcriptomics, T cell receptor (TCR) repertoires, and immunopeptidomics reveals differences between antigenic and non-antigenic tumors.** **(A)** Uniform Manifold Approximation and Projection (UMAP) of a single-cell multi-cancer transcriptomics dataset of 44308 tumor infiltrating $CD8^+$ T cells (44 patients). Tumor types included were BRCA (10932 cells), GBM (4006 cells), LUAD (18359 cells) and SKCM (11011 cells). **(B)** Threshold selection to discriminate between expanders and non-expanders at various TCR clonotype thresholds (x-axis: proportion of putative $CD8^+$ T cell expanders per cancer type, y-axis: number of isotype occurrences). 5 is the lowest threshold to distinguish between all cancer types. This cut-off results in 25083 expanders and 19155 non-expanders. **(C)** Number of unique clonotypes per cancer type between brackets, number of TCR clonotypes shared between cancer types are represented by the edge widths and listed next to corresponding edges. **(D)** The UMAP shows the positions of expander (E) and non-expander (NE) TCRs amongst $CD8^+$ T cells at a threshold of at least 5 cells with identical TCRs**. (E and F)** Signature expression (metagenes) is shown for the NeoTCR8 signature **(E)** and the cs$CD8^+$ T cell signature **(F)** in E-TCR and NE-TCR $CD8^+$ T cells. Data were analyzed using Welch's t-test. The violin plots show median and 25th-75th percentiles. **(G)** Volcano plot for the differential gene expression (DGE) analysis contrasting E-TCR versus NE-TCR $CD8^+$ T cells. **(H)** Gene set enrichment analysis (GSEA) using the REACTOME pathway dataset is shown. Significant terms are marked with a black border. **(I)** Interquartile range-scaled metagene expression is shown, representing differences in E-TCR and NE-TCR $CD8^+$ T cell signatures across each cancer type. **(J)** Hazard ratios were obtained with CoxPH survival analysis using the E-TCR and NE-TCR $CD8^+$ T cell signatures. **(K to M)** Shown is analysis of 101 immunopeptidomics studies (43306 unique linear peptides with minimal size of 8 amino acids), after quality control filtering for positive hits. Epitopes used in $CD8^+$ T cell activation assays for BLCA (29), BRCA (28), GBM (273), LUAD (191), OV (87) and SKCM (579) are presented and were annotated for antigen families including shared cancer antigens **(K)**, neoantigens **(L)** and self-antigens **(M).** Numbers

of unique epitopes are marked between brackets. **(N)** Shown is the correlation between TCR diversity (Shannon entropy value) for each cancer type and the indicated T cell signatures. The analyses were restricted to patients with a high SNV neoantigen load (above the median cut-off).

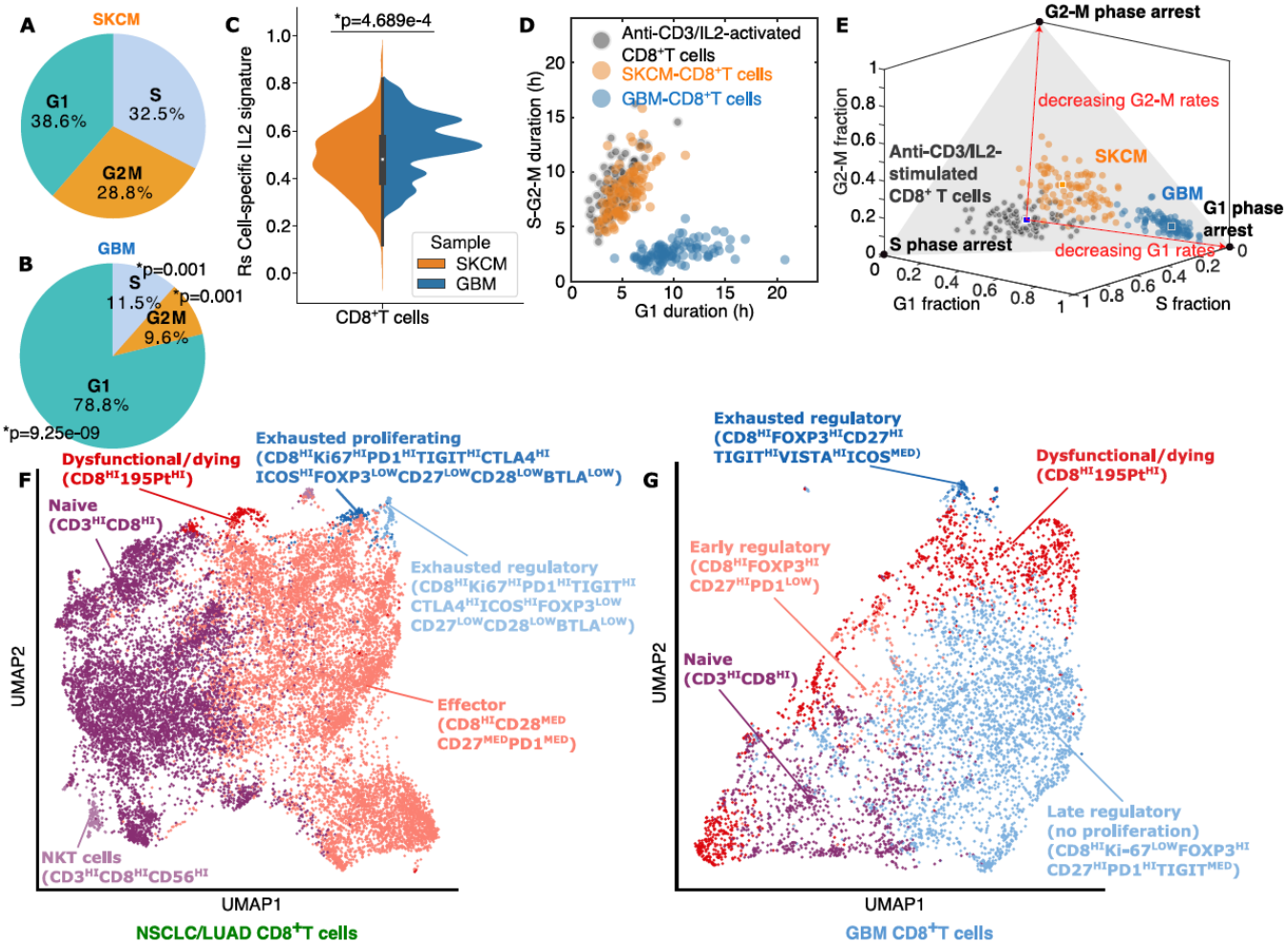
A
SKCM
G1
38.6%
S
32.5%
G2M
28.8%
B
GBM
S
11.5%
G2M
9.6%
G1
78.8%
*p=0.001
*p=0.001
*p=9.25e-09
C
*p=4.689e-4
Rs Cell-specific IL2 signature
CD8+T cells
Sample
SKCM
GBM
D
Anti-CD3/IL2-activated CD8+T cells
SKCM-CD8+T cells
GBM-CD8+T cells
S-G2-M duration (h)
G1 duration (h)
E
G2-M phase arrest
decreasing G2-M rates
Anti-CD3/IL2-stimulated CD8+ T cells
SKCM
GBM
G1 phase arrest
S phase arrest
decreasing G1 rates
G2-M fraction
G1 fraction
S fraction
F
Dysfunctional/dying (CD8HI195PtHI)
Exhausted proliferating (CD8HIKi67HIPD1HITIGITHICTLA4HI ICOSHIFOXP3LOWCD27LOWCD28LOWBTLALOW)
Naive (CD3HICD8HI)
Exhausted regulatory (CD8HIKi67HIPD1HITIGITHI CTLA4HICOSHIFOXP3LOW CD27LOWCD28LOWBTLALOW)
Effector (CD8HICD28MED CD27MEDPD1MED)
NKT cells (CD3HICD8HICD56HI)
UMAP2
UMAP1
NSCLC/LUAD CD8+T cells
G
Exhausted regulatory (CD8HIFOXP3HICD27HI TIGITHIVISTAHICOSMED)
Dysfunctional/dying (CD8HI195PtHI)
Early regulatory (CD8HIFOXP3HI CD27HIPD1LOW)
Naive (CD3HICD8HI)
Late regulatory (no proliferation) (CD8HIKi-67LOWFOXP3HI CD27HIPD1HITIGITMED)
UMAP2
UMAP1
GBM CD8+T cells
H
Effector
GPR171
FASLG
CD8A
KLRK1
SH2D1A
CCR5
CRTAM
IFNG
KLRD1
Immune checkpoints/IRs
HLA-E
ARHGDIB
LGALS9C
SLC15A3
GPBAR1
LGALS9
IFT57
PDE4B
GKAP1
ACVR2A
CD47
TNF superfamily/Inflammation
LTA
TNF
TNFSF9
TNFRSF1A
CD70
LTB
CD1C
CDKN1A
LTBR
SPRR3
SLC6A15
ACVR2B
CEACAM5
SKCM
FGFR2
FGF2
SPP1
FGFR1
TMEM30B
POSTN
RNF157
FOXQ1
RBMS3
FOXO1
SNED1
MCHR1
FZD10
LAMC1
Wound healing
J
Normalized ratio of TGF-β response/wound healing to CD8+ T cell fraction
*p=9.32e-07
*p=7.55e-14
*p=9.99e-16
*p<1.00e-16
*p<1.00e-16
SKCM
BLCA
LUAD
OV
BRCA
GBM
I
Inflammation/Tissue repair
TGF-ß response/wound healing
IL18R1
CXCL1
IL1R1
AREG
DUSP1
TNFSF9
CCL3L1
IL1R2
CCL20
ZFP36
CSF2RA
CCL3
CCL4
IFNGR1
FOS
EVI2A
OTUD1
OSM
GPR34
IL18
TNF
CCL4L2
CCR1
CCR5
TGFB1
CYP19A1
IL1A
GRN
ALOX5AP
SPP1
CLEC2D
BCL2A1
THUMPD2
C2orf27A
KLRC2
KLRC3
KLRK1
SLC1A1
GBM

**Figure 4. Cell cycle arrest and wound-healing signatures are enriched in GBM CD8$^+$ T cells. (A and B)** The pie charts represent the distribution of CD8$^+$ T cells per cell cycle phase scores (G1, S or G2M) for SKCM **(A)** or GBM **(B)** (Fisher exact test-based statistics were estimated for SKCM versus GBM comparisons for each phase score). **(C)** The fused violin-plot compares the Spearman Rho-value distribution (Y-axis) for each cell in GBM (52 cells) and SKCM (1180 cells) T cell populations (x-axis) to the T cell-specific IL-2 withdrawal signature (Welch t-test). **(D and E)** Shown is the distribution of cell cycle phase pseudo-durations for 100 CD8$^+$ T cell cycle iterations using the stretched cell cycle model **(D)** or the Erlang cell cycle model **(E)**. Red arrows in **(E)** indicate underlying mathematical reaction-rates corresponding to each (adjustable) cell cycle phase pseudo-durations and boxes represent the centre of the population. **(F and G)** Shown are UMAPs visualizing CD8$^+$ T cell populations in CyTOF datasets for non-small cell lung cancer (NSCLC) or LUAD **(F)** and GBM **(G)**. **(H and I)** Shown is network topology of SKCM **(H)** and GBM **(I)** scRNA-seq based CellPhoneDB interaction predictions, filtered based on TCGA tumor bulk RNA-seq data (threshold: FDR adjusted p-value<0.05). **(J)** The bar-plots illustrate the normalized ratio of TGF-β response and wound-healing signatures to the deconvoluted CIBERSORT-CRI CD8$^+$ T cell fraction. Statistical significance was tested with the Kruskal-Wallis test (Dunn's posthoc test for pairwise comparisons vs SKCM with Holm-sidak as posthoc, $P < 0.05$ for significance) as (GBM, n=134; BRCA, n=1088; LUAD, n=528; BLCA, n=406; SKCM, n=451; OV, n=394).

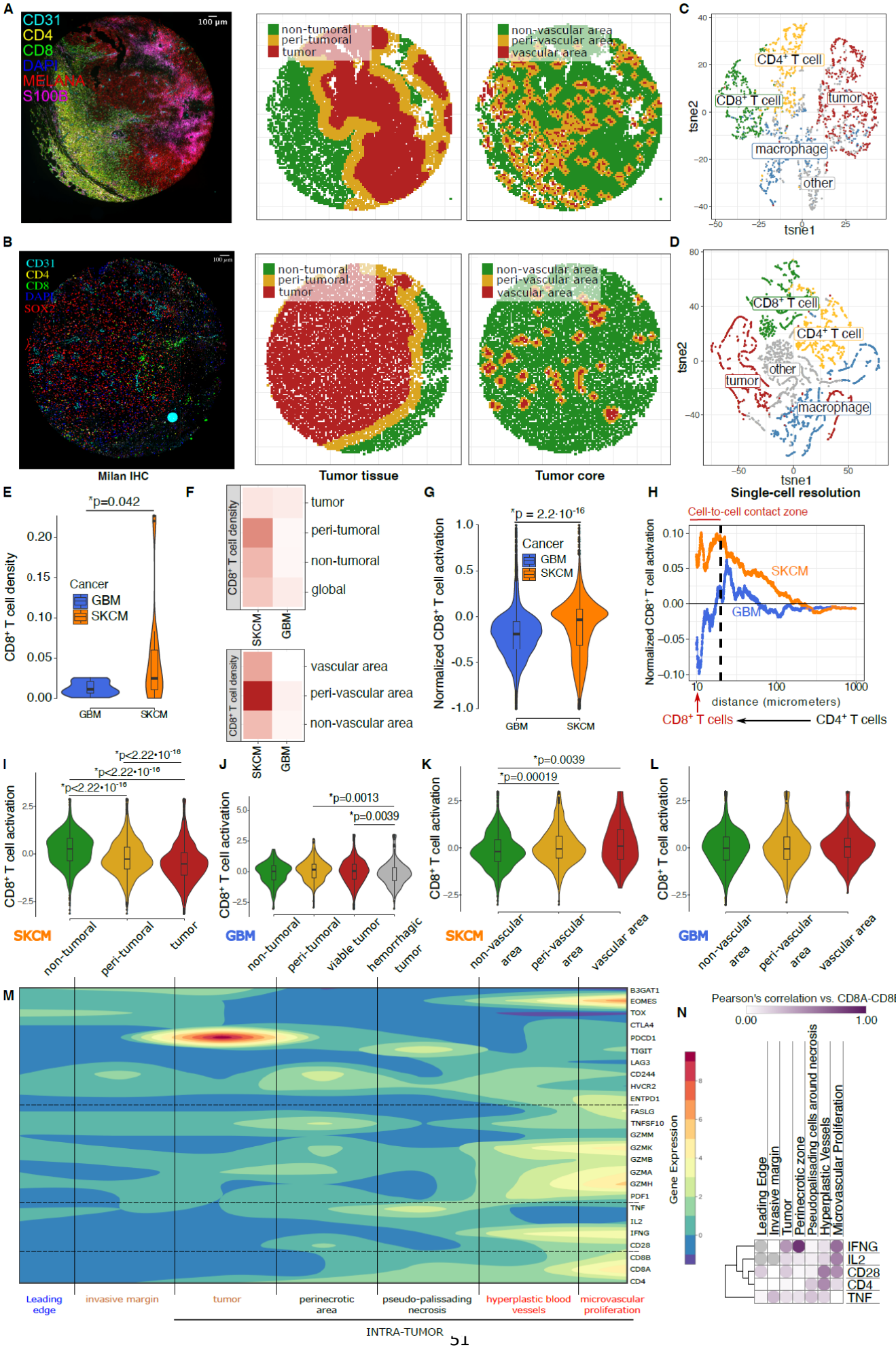
A
CD31
CD4
CD8
DAPI
MELANA
S100B
100 µm
non-tumoral
peri-tumoral
tumor
non-vascular area
peri-vascular area
vascular area
C
CD4+ T cell
CD8+ T cell
tumor
macrophage
other
tsne1
tsne2
B
CD31
CD4
CD8
DAPI
SOX2
Milan IHC
Tumor tissue
Tumor core
D
CD8+ T cell
CD4+ T cell
other
tumor
macrophage
Single-cell resolution
E
*p=0.042
CD8+ T cell density
Cancer
GBM
SKCM
F
CD8+ T cell density
tumor
peri-tumoral
non-tumoral
global
vascular area
peri-vascular area
non-vascular area
G
*p = 2.2·10-16
Normalized CD8+ T cell activation
H
Cell-to-cell contact zone
Normalized CD8+ T cell activation
SKCM
GBM
distance (micrometers)
CD8+ T cells
CD4+ T cells
I
*p<2.22•10-16
CD8+ T cell activation
SKCM
non-tumoral
peri-tumoral
tumor
J
*p=0.0013
*p=0.0039
CD8+ T cell activation
GBM
non-tumoral
peri-tumoral
viable tumor
hemorrhagic tumor
K
*p=0.0039
*p=0.00019
CD8+ T cell activation
SKCM
non-vascular area
peri-vascular area
vascular area
L
CD8+ T cell activation
GBM
non-vascular area
peri-vascular area
vascular area
M
B3GAT1
EOMES
TOX
CTLA4
PDCD1
TIGIT
LAG3
CD244
HVCR2
ENTPD1
FASLG
TNFSF10
GZMM
GZMK
GZMB
GZMA
GZMH
PDF1
TNF
IL2
IFNG
CD28
CD8B
CD8A
CD4
Leading edge
invasive margin
tumor
perinecrotic area
pseudo-palissading necrosis
hyperplastic blood vessels
microvascular proliferation
INTRA-TUMOR
N
Pearson's correlation vs. CD8A-CD8B
0.00
1.00
Gene Expression
Leading Edge
Invasive margin
Tumor
Perinecrotic zone
Pseudopalisading cells around necrosis
Hyperplastic Vessels
Microvascular Proliferation
IFNG
IL2
CD28
CD4
TNF

**Figure 5. Spatial immuno-mapping distinguishes melanoma and glioblastoma tumor tissue. (A and B)** Shown are Multiple Iterative-Labelling by Antibody-Neodeposition (MILAN)-derived representative immunofluorescent images of indicated immune and cancer cell markers in SKCM **(A, left)**, or GBM **(B, left**) tissue sections. Digital representations of indicated anatomical **(middle**) or vasculature areas **(right)** are shown for SKCM **(A)** or GBM **(B). (C and D**) tSNE maps are shown for a random subset of main annotated cell types across SKCM (n=10 samples across 10 patients) **(C)** and GBM (n=11 samples across 8 patients) **(D)**, using the same color representations as in **(A and B)**. **(E and F)** Density analysis of $CD8^+$ T cells (across entire tissue section) in GBM and SKCM is shown as violin plots **(E)** and as heatmaps showing relative distribution across indicated areas **(F)**. **(G to L)** Activation scores were calculated for each $CD8^+$ T cell based on CD69/OX40 versus LAG3/TIM3 expression. Violin plots **(G)** depict overall activation of all $CD8^+$ T cells. Line plots **(H**) show median activation of each $CD8^+$ T cell relative to its distance from nearest $CD4^+$ T cell in SKCM and GBM (for statistics, see fig. S11A and B. Activation scores of $CD8^+$ T cells were defined across indicated tumor **(I and J)** and vasculature regions **(K and L)** defined in SKCM **(I and K**) or GBM **(K and L)**. **(M)** Z-score expression profiles of indicated genes across the 7 GBM micro-dissected anatomical sections from IVY-GAP cohort (n=270 anatomical sections from 36 GBM patients). **(N)** Pearson's correlations are shown for the indicated genes within the $CD8^+$ T cell signature (*CD8A/CD8B*) in the IVY-GAP cohort. In **(E**, **G**, **I to L)**, Mann-Whitney tests with Holm's correction for multiple comparisons were applied (FDR-adjusted p-values are indicated). In **(F**, **K to L)**, vasculature analyses were restricted to only regions within the tumor core (non/peri-tumoral zones were excluded). All violin plots show median and 25th-75th percentiles.

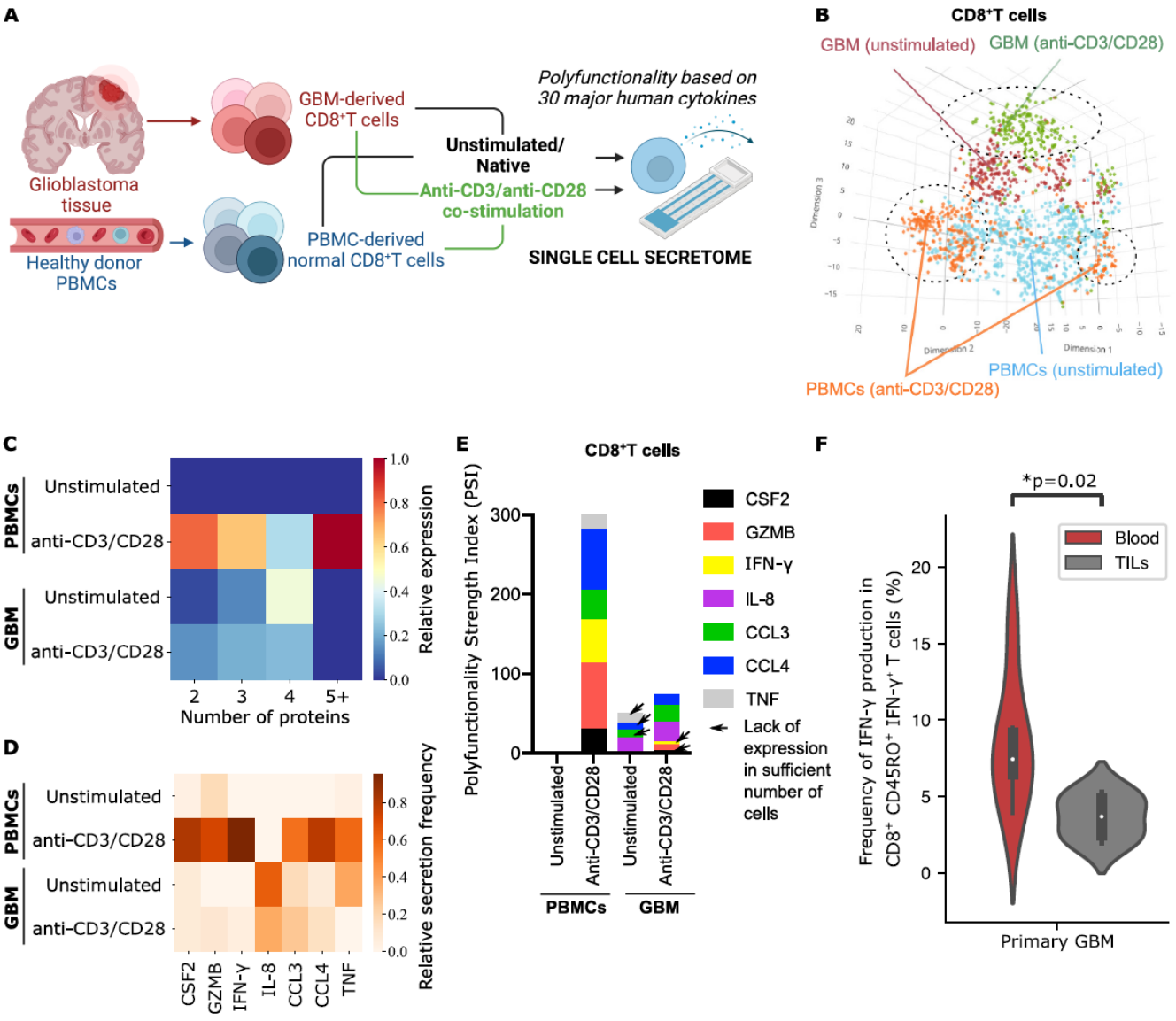


**Figure 6. Functional single-cell secretome analysis reveals tolerized-like phenotype of glioblastoma-derived CD8⁺ T cells. (A)** Shown is a visualization of the Isoplexis single-cell secretome experimental design involving GBM-derived CD8⁺ T cells (258 unstimulated versus 248 stimulated CD8⁺ T cells across 4 patients) and control peripheral blood mononuclear cells (PBMC)-derived CD8⁺ T cells (734 unstimulated versus 371 stimulated CD8⁺ T cells from 1 healthy donor). **(B**) Shown is a 3D t-SNE representation for the GBM-CD8⁺ T cells and the PBMC-CD8⁺ T cells with or without anti-CD3/CD28 stimulation. **(C**) The heatmap shows the number of unique proteins detected for respective CD8⁺ T cell populations, representing an estimation of overall polyfunctionality. **(D)** Shown are heatmaps for the individual secretion frequencies of the indicated factors. **(E)** Shown is the polyclonality strength index (PSI),

representing activity in each of the single cell secretomics samples. Colored bar sections represent the contribution of each protein to the total PSI score. Protein signals plus 3 standard deviations were calculated, and signals with signal-to-noise ratio (SNR) of at least 2 (relative to the background threshold) and from at least 20 single cells or 2% of all single cells (whichever quantity was larger) were considered substantially secreted. Signals that were insufficiently above background owing to these thresholds are denoted by an arrow. **(F)** Shown is a violin plot (median and 25th-75th percentiles) for the frequency of IFNγ-producing, $CD45RO^{+}$, GBM-derived, PBMC-associated (blood) or tumor-infiltrating $CD8^{+}$ T cells (TIL) after stimulation with ionomycin/PMA and analyzed by flow cytometry (n=6; Mann-Whitney t-test).

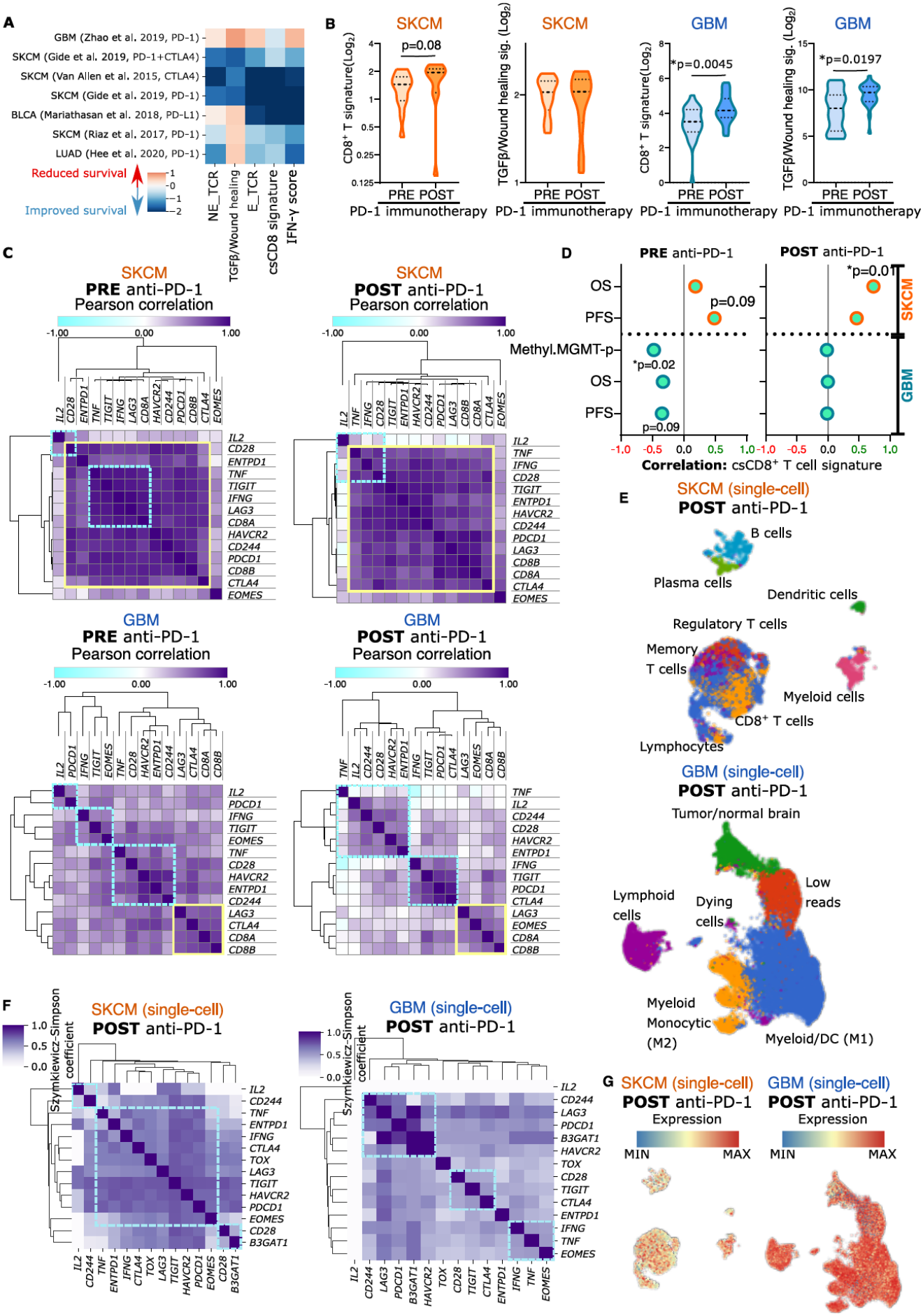
A
GBM (Zhao et al. 2019, PD-1)
SKCM (Gide et al. 2019, PD-1+CTLA4)
SKCM (Van Allen et al. 2015, CTLA4)
SKCM (Gide et al. 2019, PD-1)
BLCA (Mariathasan et al. 2018, PD-L1)
SKCM (Riaz et al. 2017, PD-1)
LUAD (Hee et al. 2020, PD-1)
Reduced survival
Improved survival
NE_TCR
TGFβ/Wound healing
E_TCR
csCD8 signature
IFN-γ score
B
SKCM
GBM
p=0.08
*p=0.0045
*p=0.0197
CD8+ T signature(Log2)
TGFβ/Wound healing sig. (Log2)
PRE POST
PD-1 immunotherapy
C
SKCM
PRE anti-PD-1
Pearson correlation
SKCM
POST anti-PD-1
Pearson correlation
GBM
PRE anti-PD-1
Pearson correlation
GBM
POST anti-PD-1
Pearson correlation
D
PRE anti-PD-1
POST anti-PD-1
OS
PFS
Methyl.MGMT-p
p=0.09
*p=0.02
*p=0.01
SKCM
GBM
Correlation: csCD8+ T cell signature
E
SKCM (single-cell)
POST anti-PD-1
B cells
Plasma cells
Dendritic cells
Regulatory T cells
Memory
T cells
Myeloid cells
CD8+ T cells
Lymphocytes
GBM (single-cell)
POST anti-PD-1
Tumor/normal brain
Low
reads
Lymphoid
cells
Dying
cells
Myeloid
Monocytic
(M2)
Myeloid/DC (M1)
F
SKCM (single-cell)
POST anti-PD-1
GBM (single-cell)
POST anti-PD-1
Szymkiewicz-Simpson coefficient
G
SKCM (single-cell)
POST anti-PD-1
GBM (single-cell)
POST anti-PD-1
Expression
MIN
MAX

**Figure 7. Immunogenomics associate with outcomes of immuno-oncology clinical trials.** **(A)** The heatmap shows CoxPH regression Z-scores for single-cell TCR signatures, TGF-β/wound-healing signatures, $CD8^+$ T cell signatures and *IFNG* signatures in 7 distinct clinical trials covering 474 patients. **(B to G)** Clinical trials involving pre and post anti-PD-1 treatment-derived tumor-tissue from SKCM (Pre, n=13; Post, n=11, 11 longitudinal) or GBM (Pre, n=24; Post, n=25, 0 longitudinal) were analyzed. **(B)** Violin plots for scores pre- and post-immunotherapy for indicated signatures are shown for the indicated tumor types (data were analyzed by Mann-Whitney test). **(C)** Correlation matrices are shown for the $csCD8^+$ T cell-signature in these trials. Yellow squares indicate the cluster marked by *CD8A/B* genes, blue squares illustrate clusters consisting of effector genes (*IFNG*, *IL2*, *TNF, CD28*). **(D)** Shown are Pearson correlations between $csCD8^+$ T cell-signature and patient outcomes [OS, PFS, and O6-methylguanine-DNA methyltransferase, (MGMT) promoter-methylation (Methyl.MGMT-p)]. **(E)** UMAPs of the cell composition in scRNA-seq datasets from patients with SKCM (E, upper panel) and GBM (E, lower panel) treated with ICBs. **(F)** Heatmap visualizations of the correlation between $csCD8^+$ T cell signature genes in $CD8^+$ T cells recovered post-treatment with anti-PD-1 and anti-CTLA-4 in SKCM (F, left) or anti-PD-1 ICB in GBM (F, right). **(G)** TGF-β/wound-healing signature expression is overlaid on the UMAP representation for SKCM (G, left) and GBM (G, right). Violin plots show median and 25th-75th percentiles.

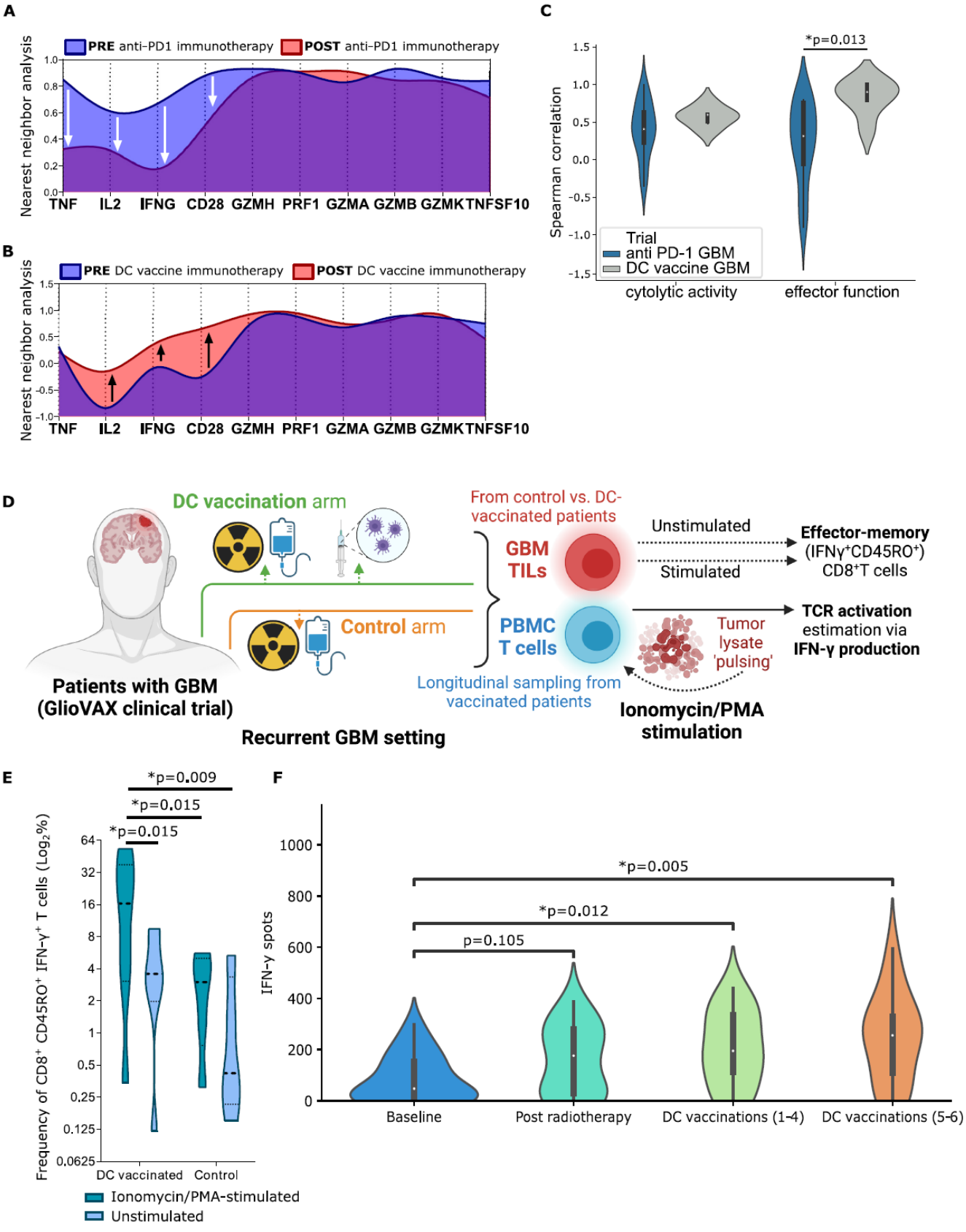
A
PRE anti-PD1 immunotherapy
POST anti-PD1 immunotherapy
Nearest neighbor analysis
TNF IL2 IFNG CD28 GZMH PRF1 GZMA GZMB GZMK TNFSF10
B
PRE DC vaccine immunotherapy
POST DC vaccine immunotherapy
Nearest neighbor analysis
TNF IL2 IFNG CD28 GZMH PRF1 GZMA GZMB GZMK TNFSF10
C
*p=0.013
Spearman correlation
Trial
anti PD-1 GBM
DC vaccine GBM
cytolytic activity
effector function
D
DC vaccination arm
Control arm
Patients with GBM
(GlioVAX clinical trial)
Recurrent GBM setting
From control vs. DC-vaccinated patients
GBM TILs
PBMC T cells
Unstimulated
Stimulated
Effector-memory (IFNγ+CD45RO+) CD8+T cells
TCR activation estimation via IFN-γ production
Tumor lysate 'pulsing'
Longitudinal sampling from vaccinated patients
Ionomycin/PMA stimulation
E
*p=0.009
*p=0.015
*p=0.015
Frequency of CD8+ CD45RO+ IFN-γ+ T cells (Log2%)
DC vaccinated
Control
Ionomycin/PMA-stimulated
Unstimulated
F
IFN-γ spots
*p=0.005
*p=0.012
p=0.105
Baseline
Post radiotherapy
DC vaccinations (1-4)
DC vaccinations (5-6)

**Figure 8. DC vaccination facilitates effector immunity against glioblastoma in clinical trials. (A and B)** Tissues from clinical trials involving DC vaccination (Pre, n=6; Post, n=6, 6 longitudinal) or anti-PD-1 treatment (Pre, n=24; Post, n=25, 0 longitudinal) in GBM were used to create cubic-spline representations of nearest-neighbor (Pearson's correlation) analyses for indicated genes. Nearest neighbor analyses were conducted with data from a GBM anti-PD-1 immunotherapy trial **(A**) and the DC vaccination trials **(B**). 1000-permutations for initial candidate selection were used to approximate the optimal results. **(C)** Violin plots are shown comparing the correlations between pre- and post-treatment expression of genes involved in a cytolytic activity signature (*PRF1, GZMA, GZMB, GZMH, GZMK, TNFSF10*) and an effector function signature (*IFNG, IL2, CD28*). Data are from clinical trials employing anti-PD-1 treatment (n=25) and DC vaccination (n=6) for GBM. **(D)** Shown is a schematic overview of the GlioVax clinical trial and the experimental design. **(E)** Violin plots show the frequency of IFN-γ-producing GBM-derived effector-memory $CD8^+$ T cells. Cells were either stimulated with PMA/ionomycin or left unstimulated and were from either the DC vaccination arm (n=7) or control arm (n=5) at suspected tumor recurrence. Cells were analyzed by flow cytometry. Data were analyzed with a one-way ANOVA. **(F)** Violin plot is shown for the number of IFN-γ spots produced by PBMCs collected longitudinally from patients at different vaccination timepoints (baseline, n=18; post-radio-chemotherapy/RC or pre-vaccination, n=18; post DC vaccinations 1-4, n=18; post DC vaccinations 5-6, n=17). PBMCs were pulsed with corresponding GBM-tumor lysate-loaded DC and analyzed for IFN-γ production by ELISPOT (Kruskal-Wallis test, Dunn's posthoc for pairwise comparison, $p < 0.05$ for significance). The violin plots show median and 25th-75th percentiles.